INTERNATIONAL JOURNAL OF Telecommunications
AIR DEFENSE COLLEGE

Investigation and Implementation of Integrated SIW System for Hexagonal Diamond of Lamda Shape Slots Fractal Array Antenna for X and KU-Band Applications

Ahmed F. Miligy[1,*], Assem H. Elfeky[2], Hassan Nadir Kheirallah[3] and Mohamed R. M. Rizk[4]

Citation: Miligy, A. F.; Elfeky, A. H.; Kheirallah, H. N.; Rizk, M. R. M. *International Journal of Telecommunications, **IJT'2021**, Vol. 01, Issue 01, pp. 1-25, December 2021.* https://ijt-adc.org/articles/2805-3044/576196

Editor-in-Chief: Yasser M. Madany
Received: 28-10-2021
Accepted: 9-12-2021
Published: 22-12-2021

Publisher's Note: The International Journal of Telecommunications, IJT, stays neutral regarding jurisdictional claims in published maps and institutional affiliations.

[1] Communication and Electronics Department, ADC, Alexandria University, Alexandria, Egypt; ahmed_miligy73@yahoo.com
[2] Communication and Electronics Department, ADC, Alexandria University; Alexandria, Egypt; asem.hussein@alexu.edu.eg
[3] Department of Electrical Engineering, Alexandria University, Alexandria 21526, Egypt; engyk@dataxprs.com.eg
[4] Department of Electrical Engineering, Alexandria University, Alexandria, Egypt; mohamed.rizk@alexu.edu.eg
* Correspondence: ahmed_miligy73@yahoo.com.

Abstract: This paper introduces an investigation and implementation of integrated SIW system using Rogger RT/duriod 5880 substrate of $\varepsilon_r = 2.2, \tan\delta = 0.0009$ and thickness 0.79 mmsimulated using HFSS. The proposed system is an integration of three main microwave devices: SIW divider/combiner taking a shape of wraparound rhombic with two isolated output ports, SIW phase shifter and two arrays of SIW hexagonal diamond of lamda shape slots fractal antenna. The divider operates efficiently in five wide bands [(9.7-11.36)/ (11.84-12.35)] GHz and [(13.5-14.05)/ (14.55-15.46)/ (15.62-16.7)] GHz for X and KU-Band applications respectively. The divider feeds two arrays of SIW fractal array antenna of hexagonal shape; one of them has a phase shifted input using SIW phase shifter. The proposed system is based on SIW technology to meet the requirement of multiple frequency bands for x-band missile guidance, KU-band satellite altimetry and wireless communication system applications. The measurement results have been obtained in laboratory using (R&S ZVB 20 vector network analyzer 10 MHz: 20 GHz) with agreement between about 11 resonance operating frequencies of the radiating antenna for both simulated and measured results. For one watt incident power the obtained antenna parameters were found to be $S_{11} = -43\ dB$, U=0.72 W/Str., accepted power=0.99 W, radiated power=0.98 W, absolute directivity, D =9.7, absolute gain, G =7.1 and radiation efficiency = 98% at f = 13.7 GHz as the most agreement frequency point between simulation and implementation results.

Keywords: Substrate integrated waveguide; SIW divider/combiner; SIW slot antenna; SIW phase shifter; fractal antennas

1. Introduction

The rectangular waveguide devices manufacturing is rather complicated and more expensive since high precision mechanical adjustment is needed to obtain the resonant in case of slots at the standing wave peaks. Moreover, the integration of these structures with planar components are more difficult and requires sophisticated transitions [1-3]. However, Microstrip technologies are, easy and less expensive compared with waveguide technologies, but have the disadvantages of radiation loss and not being shielded [4-7]. A construction of metal filled via-hole arrays in substrate and grounded planes is the so-called substrate integrated waveguide

(SIW) technology which can be easily integrated with other elements on a single substrate for systems connection. These systems can be miniaturized into small package of compact size and less cost. It can therefore be fabricated using dielectric substrate materials. So, the SIW has wide applications in the design of millimeter-wave and microwave devices due to its loss transmission characteristic, compact size, flexibility in the realization of microwave circuits which require a good quality factor and low cost [8-10]. Many devices and components for rectangular waveguide technologies can be analyzed, designed, and implemented using SIW such as, dividers, combiners, circulators phase shifters and tee planes, slot antennas and other microwave devices and components making them simpler to build, lighter, and less expensive than a waveguide device, this is due to the close similarity of dispersion and propagation characteristics of both technologies. The SIW phase shifters, dividers, coupler, junctions, circulators, and other microwave components are vital devices in radar system applications. Phase shifters are essential for array antenna applications for beam steering using different techniques. Power dividers are passive microwave device used for power division or power combining. In power division, an input signal is divided into more signals of lesser power. Three-port divider take the form of T-junctions and other forms, while four-port networks take the form of directional couplers and hybrids. Power dividers are often 3-dB type for equal division. All these structures can be designed, analyzed, and implemented using SIW technologies [11-13].

The progress and development of wireless, satellite communication and military systems and their applications is taking place all over the world. Wideband, multiband, lower price, ease of fabrication and small size antenna are main objectives for these applications due to their advantages. Fractal antennas are important arrays required to cover these demands. Fractal antenna has a non-regular and never-ending pattern structures depending on repetition of single patterns over in ongoing feedback loop. Fractal antennas are differing from traditional antennas, and they resolve two limitations. The first is the dependence upon the electrical dimensions of the antenna as an antenna parameter. The second is that the size of the antenna is reduced by increasing the effective length of fractal structure. Fractal antenna has the advantages of compact size, impedance matching, wideband, multiband, and constant efficiency over large band. However, they have disadvantages of loss in gain, numerical limitations and the benefits begin to decrease after first iteration.

The proposed fractal antenna system can be operated in different frequencies. The obtained frequencies are in the X and Ku- band. The different applications of the proposed antenna system in X-band are Military applications like missile guidance, marine radar systems, air-borne tracking and government applications like remote detecting, versatile systems administration, and airborne insight, observation, and surveillance (AISR) which rely on government and business satellite frameworks. For Ku-band, which is essentially utilized for satellite interchanges, Fixed satellite service (FSS) like television transmission, Broadcast Satellite Service (BSS) like telecommunication, wireless communication, and Satellite altimetry [14-16].

2. The Basic SIW and Rectangular Waveguide Structures

Due to advantages of SIW technology, especially the minimal radiation loss for high frequency, compact size and easy integration with planar structures, it is considered an important and new technology for microwave integrated circuits applications. The SIW is considered a quasi-rectangular waveguide (RW) as it is a dielectric filled structure with low conducting of (cylindrical or rectangular) via rows instead of metallic walls. Cylindrical via arrays are the common in use with diameter d and pitch p between each via where d must be less than p, $(d < P)$ as $p < 4d$and$p < \frac{\lambda_0}{2}\sqrt{\varepsilon_r}$ [11-13]. The physical dimensions of SIW structure determine the propagating$TE_{n,0}$mode, n=1, 2, with minimal loss. The dominantTE_{10}has minimum cutoff frequency and maximum handling power with vertical electric current density on via rows. However, due gaps separation between via rows the TM modes cannot be supported in SIW structures because of the strong radiation of longitudinal surface current. The cutoff frequency of $TE_{m,n}$ mode in the traditional rectangular waveguide can be calculated using (1) where, m and n are the number of half waves in x and y direction considering z as the direction of wave propagation. For the TE_{10} mode calculations equation(1) is reduced to (2) for the air filled waveguide[17], where c is the free space velocity of light ($c = 3 \times 10^8\ m/s$).So, the dimension $a = 24.39\ mm$ for TE_{10} air filled waveguide, at $f_c = 6.15\ GHz$,is the cut off frequency of propagating mode and operating frequency must be more than f_c.

$$f_{c_{TEm,n}} = \frac{\upsilon}{2}\sqrt{\left(\frac{m}{a}\right)^2 + \left(\frac{n}{b}\right)^2} \quad (1)$$

$$f_c = \frac{c}{2a} \quad (2)$$

For dielectric filled rectangular waveguide (DFW) with the same cutoff frequency the width of the (DFW) is$a_d$calculated using (3) equals 16.44 mm for TE_{10} mode. Finally the SIW width a_S=17 mm and $\lambda_{gs} = 29\,mm$ using (4) and (5) respectively with $p = 1.2\,mm$and $d = 0.8$ mm as $p < 4d$and$p < \frac{\lambda_0}{2}\sqrt{\varepsilon_r}$ [11-13].

$$a_d = \frac{a}{\sqrt{\varepsilon_r}} \quad (3)$$

$$a_s = a_d + \frac{d^2}{0.95P} \quad (4)$$

$$\lambda_{gs} = \frac{2\pi}{\sqrt{\left(\frac{2\pi f}{c}\right)^2 . \varepsilon_r - \left(\frac{\pi}{a_s}\right)^2}} \quad (5)$$

The proposed basic SIW structure without tapering transition has been designed [11-13], simulated, analyzed using HFSS simulator [18] before implemented using Rogger RT/duriod 5880 substrate of $\varepsilon_r = 2.2$, tangent loss $\tan\delta = 0.0009$ and thickness $h_R = 0.79\,mm$. The basic SIW and WG structure dimensions are illustrated in figure 1 and their dimensions are tabulated in table 1.

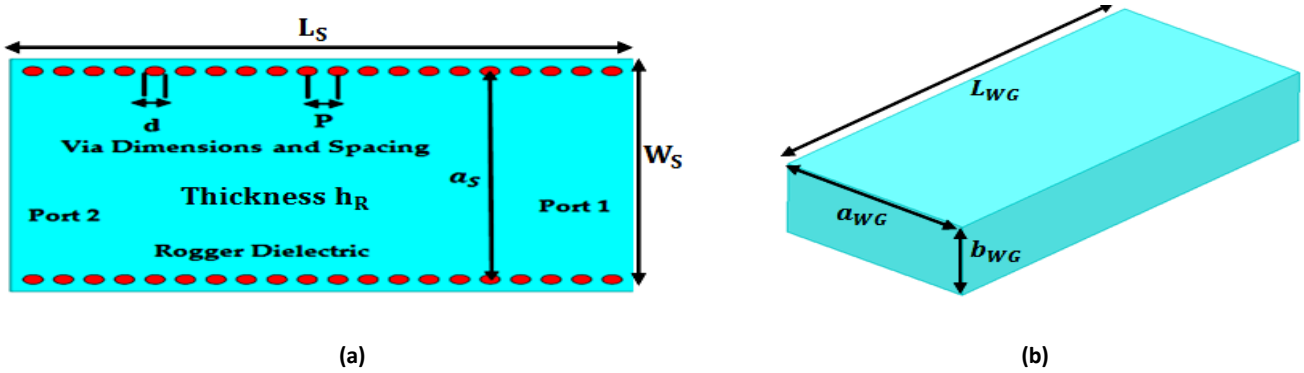

Figure 1. The Basic structures: (a) The SIW dimensions and view; (b) The rectangular waveguide dimensions and view..

Table 1. Parameters and Dimensions of the Basic Structures [mm].

Parameters of the SIW Structure									Parameters of the RW Structure				
ε_r	tanδ	h_R	λ_{gs}	W_S	$L_S = 2\lambda_{gs}$	a_S	p	d	ε_r	λ_{WG}	a_{WG}	b_{WG}	$L_{WG} = 2\lambda_{WG}$
2.2	0.0009	0.79	29	19.5	58	17	1.2	0.8	1	65.5	22.86	10.16	131

Simulation results of the proposed structures have been obtained using HFSS simulator based on the finite element method (FEM) and the simulation results are illustrated in Figure 2. The scattering matrix [19] of both structures expressed as in (6) at the minimal magnitude of reflection coefficient indicates a good performance of the structure as the transmission coefficient reaches about one magnitude all over the frequency band.

$$[S_{SIW}] = \begin{bmatrix} 0.000656 & 0.9964 \\ 0.9964 & 0.000634 \end{bmatrix} \text{ and } [S_{RW}] = \begin{bmatrix} 0.000076 & 0.998 \\ 0.998 & 0.0000776 \end{bmatrix} \quad (6)$$

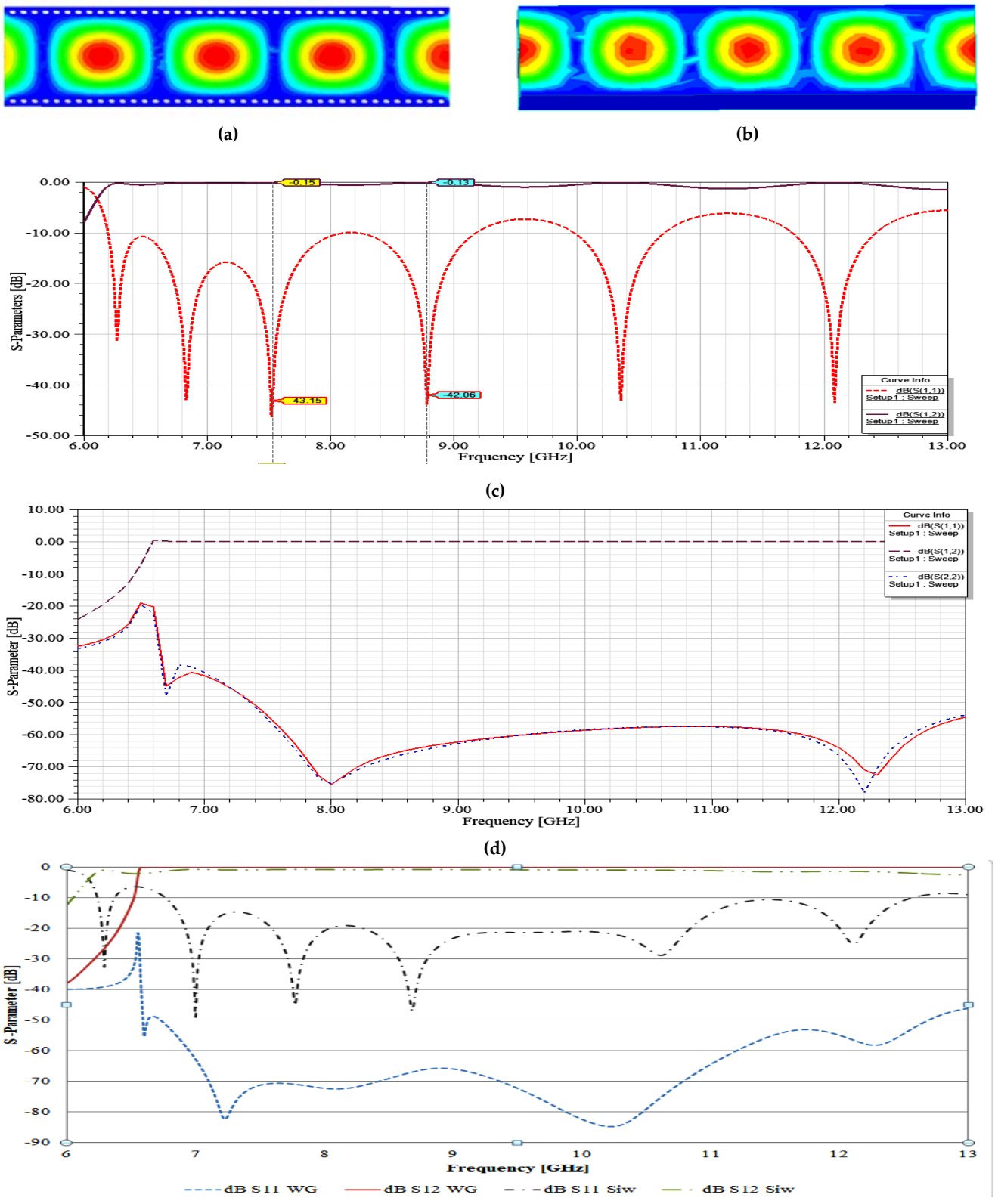

Figure 2. The basic structures simulation results: (a) The SIW electric field distribution [V/m]; (b) The RW electric field distribution [V/m]; (c) The SIW scattering parameters [dB]]; (d) The RW scattering parameters [dB]]; (e) Comparison between the SIW and RW scattering parameter simulation results [dB].

From simulation results shown in figure 2 (c and d), the scattering parameters show that both structures have a wide band transmission coefficient with minimum reflection coefficient as impedance matching network. Also

the electric field distribution for the dominant mode illustrated in figures 2 (a and b) shows an excellent distribution for the proposed structures. Figure 2 (e) presents a compression between scattering parameters for both the SIW and WG structure which indicates a good performance for each with the advantages of SIW over WG such as easy of fabrication and integration with other systems. The selection of using SIW technology has been chosen due to its easy for integration, low cost and easy for fabrication and other advantages of SIW over WG which summarized in table 2.

Table 2. Comparison between SIW and RW structures.

Parameters	Size/Integration	Cost	Connection	Power	Fabrication	Losses		S_{11}	S_{12}
RW	Large/ difficult	Expensive	Difficult using flanges	High	Difficult	**Conductor**	High	0.00076	0.998
						Dielectric	Low		
						Radiation	Low		
SIW	Compact/ Easy	Less expensive	Easy using tapering transition	Low	Easy	**Conductor**	Low	0.00065	0.99
						Dielectric	High		
						Radiation	Low		

3. The SIW-Microstrip Tapering Transition

Several techniques for transition between printed transmission lines and SIW have been proposed to match the quasi-TEM mode of Microstrip line with TE_{10} of SIW structure and their field distribution. The objective is to maintain the reflection coefficients in minimal value and hence increase the transmission coefficient without any mechanical assembly for integrated planar circuit on the same substrate [20-22].These techniques include SIW-Microstrip transition, based on taper, current probe or a 90^obend. The most common used is the Microstrip transition tapering [23-25].The width and length of the Microstrip transmission line feeding are$W_{T2} = 3.7$ mmand $L_{T2} = \frac{\lambda_{gT}}{4} 10\ mm$respectively calculated using (7) to (9) for 50 ohm impedance [17], for$\varepsilon_r = 2.2$ of and $h_R = 0.79\ mm$. The length of tapering $L_{T1} = \frac{\lambda_{gs}}{3} = 10$ mm. Calculations of tapering width section W_{T1}based on the calculation of the SIW wave impedance Z_{TE} and then calculate the ohmic resistance Z_P of SIW using (10). Finally, $W_{T1} = 4.8$ mm using (7) to (9) for calculated Z_P[20-25].

$$\frac{W_{T2}}{h_R} = \begin{cases} \dfrac{8e^{A}}{e^{2A}-2} & \text{for } \dfrac{W_{T1}}{h_R} < 2 \\ \dfrac{2}{\pi}\left[B - 1 - \ln(2B-1) + \dfrac{\varepsilon_r - 1}{2\varepsilon_r}\left(\ln(B-1) + 0.39 - \dfrac{0.61}{\varepsilon_r}\right)\right] & \text{for } \dfrac{W_{T1}}{h_R} > 2 \end{cases} \tag{7}$$

$$A = \frac{Z_0}{60}\sqrt{\frac{\varepsilon_r+1}{2}} + \frac{\varepsilon_r-1}{\varepsilon_r+1}\left(0.23 + \frac{0.11}{\varepsilon_r}\right) \text{ and } \quad B = \frac{377\pi}{2Z_0\sqrt{\varepsilon_r}} \tag{8}$$

$$\varepsilon_e = \frac{\varepsilon_r+1}{2} + \frac{\varepsilon_r-1}{2}\frac{1}{\sqrt{1+12h_R/w_{T1}}} \text{ and } \lambda_{gT} = \left(3\times 10^8/f\sqrt{\varepsilon_e}\right) \tag{9}$$

$$Z_{TE} = \sqrt{\frac{\mu}{\varepsilon}} \times \frac{\lambda_{gs}}{\lambda} \text{ and } \quad Z_P = Z_{TE}\frac{\pi^2 h_R}{8a_S} \tag{10}$$

The proposed basic SIW structure with tapering transition has been designed; analyzed, simulated using HFSS and implemented using Rogger RT/duriod 5880 substrate of $\varepsilon_r = 2.2$, tangent losstan $\delta = 0.0009$ and thickness $h_R = 0.79\ mm$shown in figure 3 and dimensions are tabulated in table 3.

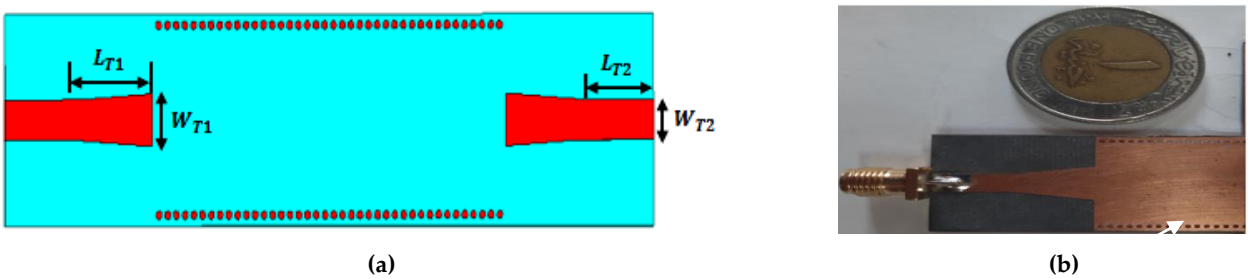

(a) **(b)**

Figure 3. The basic SIW with tapering transition: (a) The inner dimensions and view; (b) The implemented SIW-Microstrip tapering transition.

Table 3. Dimensions of the Basic SIW-Microstrip Transition Structure [mm].

Dimensions of the SIW-MicrostripTransition Structure				
λ_{gT}	W_{T1}	W_{T2}	L_{T1}	$L_{T2} = \frac{\lambda_{gT}}{4}$
40	4.8	3.7	10	10

Simulation results for the proposed SIW-Microstrip transmission shown in figure 4 using HFSS has been obtained. Figure 4(a) show the scattering parameters in dB which show that the reflection coefficient is more or less than -10 dB and reaches to about -50 dB at some frequencies. The transmission coefficient is close to -0.3 dB due to conductor and dielectric loss of designed material over the most of the operating frequency band.

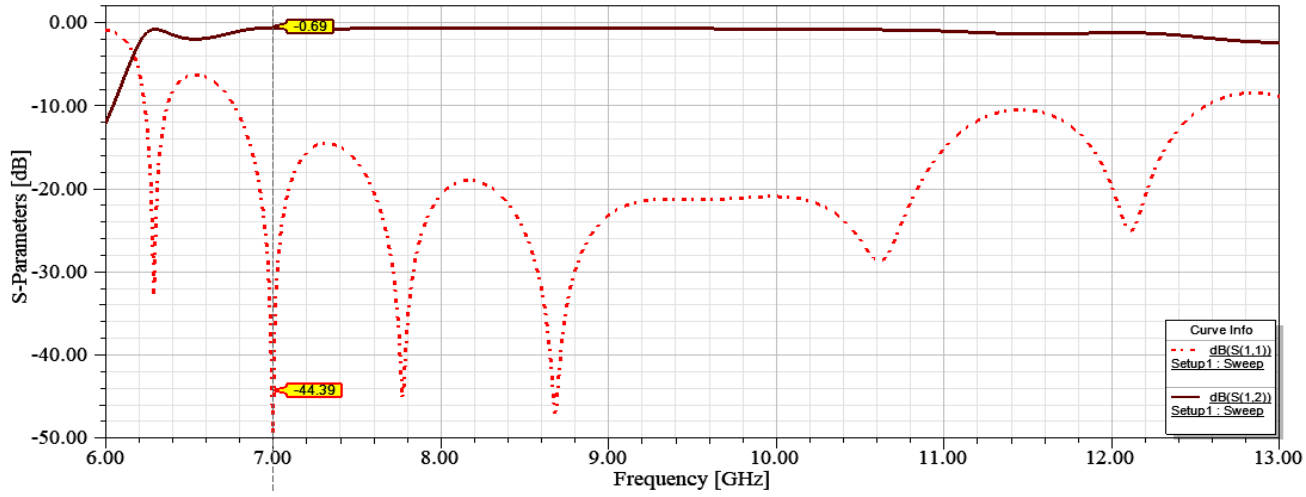

(a)

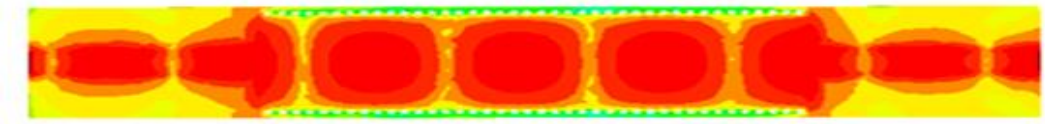

(b)

Figure 4. The SIW-Microstrip transition simulation results: (a) The S-parameters [dB]; (b) The electric field distribution [V/m].

As a conclusion for tapering transition, the S_{11} remains below -10 dB and over most of the frequency band and the S_{12} and $S_{21}$is around - 0.3 dB across the entire band. Without any mechanical assembly this concept allows

the design of integrated planar circuit of Microstrip and SIW on the same substrate. The electric field distribution which indicates the good performance of the structure is shown in figure 4 (b).

4. The SIW Phase Shifter

Phase shifters are essential and vital component in microwave system as they shift the phase of the electrical signal of different applications such wireless communications, biomedical, instrumentation systems and radar systems. One of the most important applications in radar systems is the phased antenna arrays to adjust the phase of signal feeding elements of array for beam steering [26-30]. The SIW phase shifter may be able to be obtained using different techniques. One of these techniques is by using SIW transmission structures with a number of embedded metallic via as a cylindrical inductive post in a specific position of the structure. The inductive posts are equivalent to a network of high pass filter [31-34]. The equivalent circuit of two metal posts expressed as T-network with two reactance's jX and susceptance jB.The values of equivalent circuit depend on and vary with both the diameter and position of metal posts in the SIW transmission structure. To obtain a phase advance in phase shifter systems, a high pass filter may be used as the switched high-pass/low-pass [34-37]. The phase shift φ, of the high-pass filter expressed in (11) [26] indicate the dependence of the phase shift on the diameter and position of the embedded metallic via.

$$\varphi = \tan^{-1}\left[\frac{\mathrm{B} + 2\mathrm{X} - \mathrm{BX}^2}{2(1 - \mathrm{BX})}\right] \tag{11}$$

Another technique is using a row of metallic via in the SIW line to change the phase of the incident wave by means of changing their position in substrate dielectric of SIW structure [30-37]. The main structure and implemented view of the SIW phase shifter is shown in figure 5 (a), its dimensions tabulated in table 4 and simulation results are shown in Figure 5 (b-e).

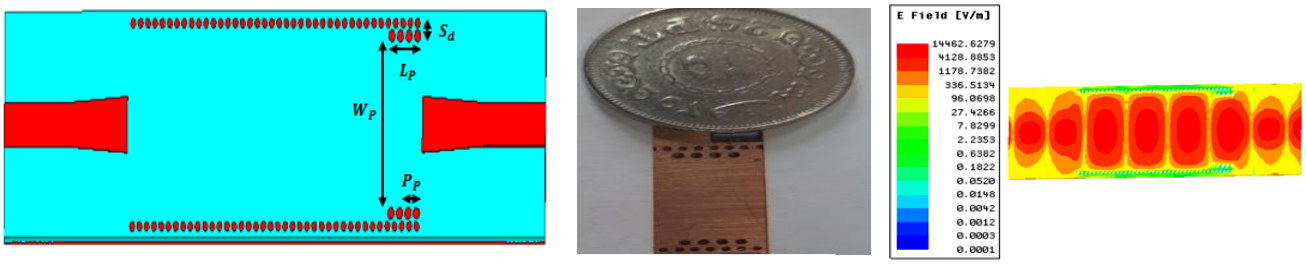

(a) **(b)**

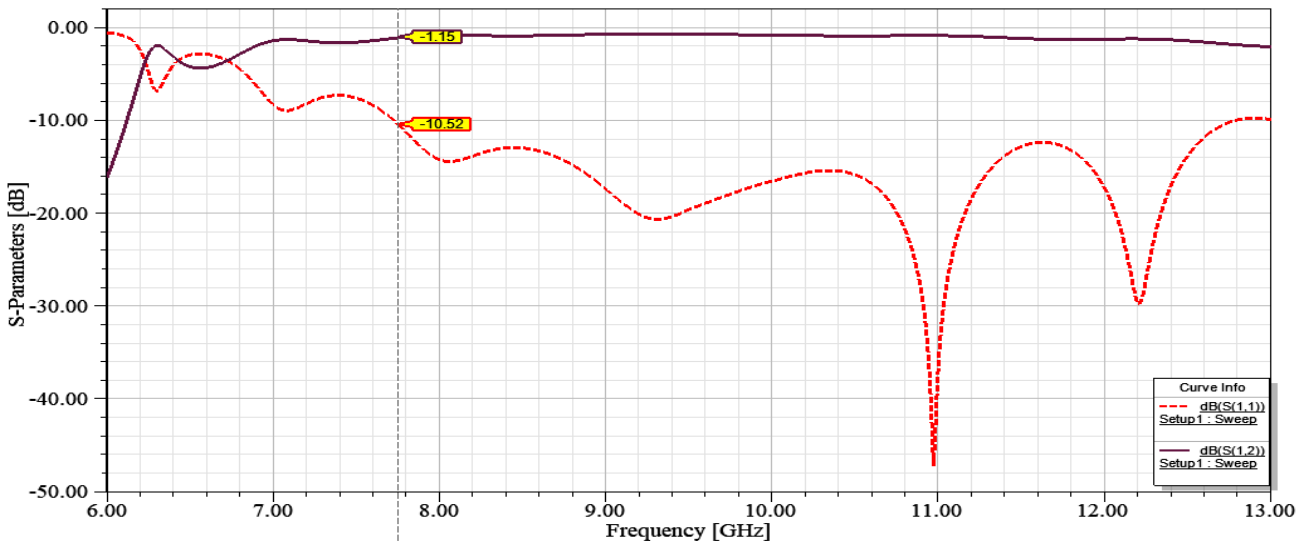

(c)

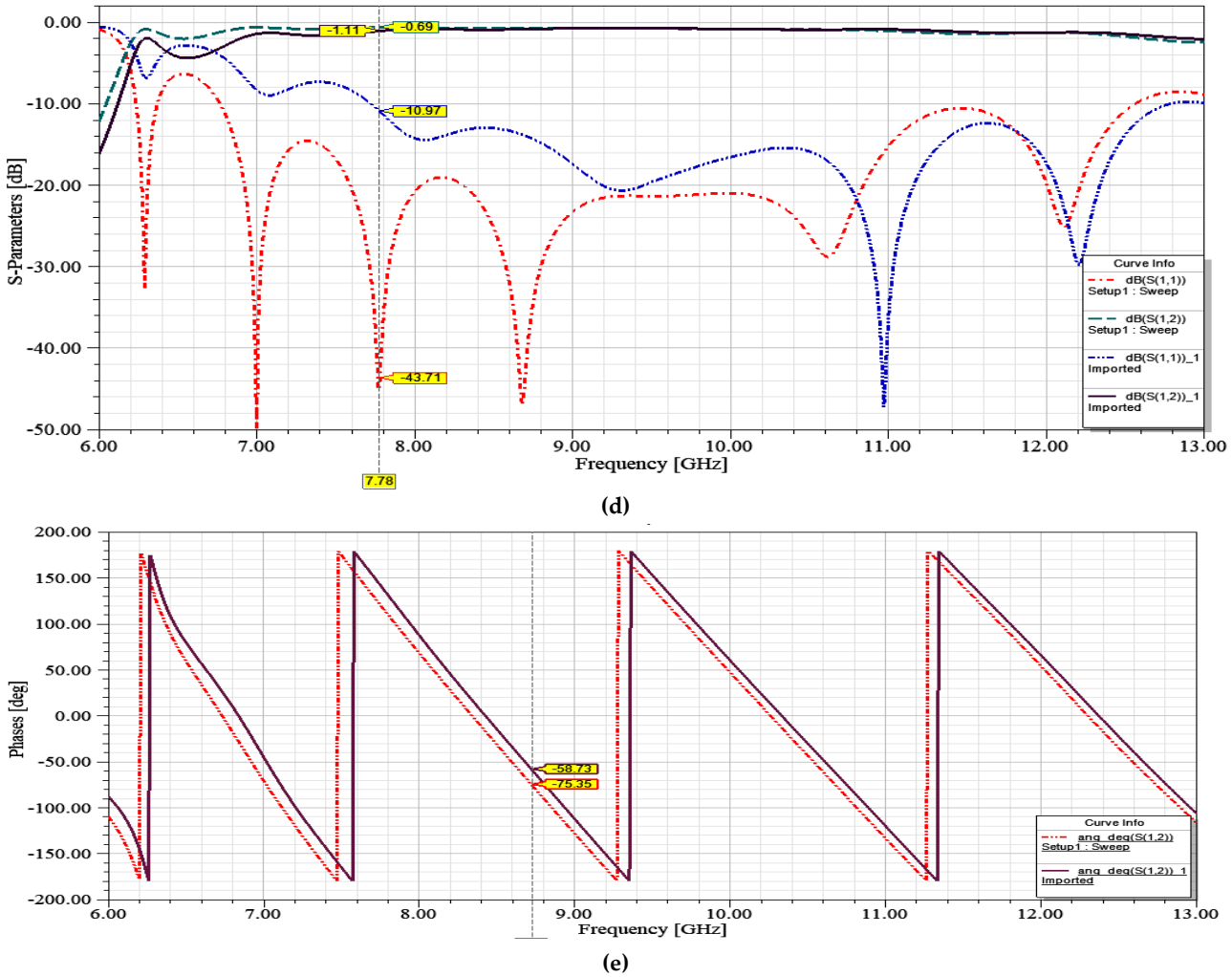

Figure 5. The SIW phase shifter structure and simulation results: (a) The SIW inner dimensions and implemented view; (b) The SIW electric field distribution [V/m]; (c) The scattering parameters [dB]; (d)The S-parameters of SIW without and with phase shifter [dB]; (e) The phase shift angle [deg.].

Table 4. Dimensions of the SIW Phase Shifter Structure [mm].

Dimensions of the SIW Phase Shifter Structure			
S_d	L_P	W_P	P_P
1.1	5.2	15.3	1.4

Figure 5 (c) shows the scattering parameters of the SIW phase shifter and from the results it is found that the transmission coefficient is about -0.1 dB with reflection coefficient less than -10 to -50 dB over most of the frequency band from 6-13 GHz especially at 11 GHz. Comparison between the basic SIW without and with phase shifter is shown in figure 5 (d and e). Results shown in figure (e), confirms the phase change between ports for array antenna feeding applications. Figure 5 (d) shows the comparison of scattering parameters of the SIW without and with phase shifter which results in transmission all over band with minimum reflection coefficient. The electric field distributions [V/m] of the structure in figure 5 (b) shows the performance of the structure and determine how the design works.

5. The New Shape of SIW Rhombic Wraparound Divider/Combiner

Power dividers are considered one of the microwave circuit components which are used in different applications such multiplexers, couplers and antenna systems. The power dividers are used to equally split signal power in a system. The Low loss capacity and high quality factor can be obtained using rectangular waveguide

power divider for microwave applications but the high cost and volume are drawbacks of this technology. Microstrip technologies overcome the drawback of cost and volume, but, still have a disadvantage of high radiation loss which limits using these technologies in different applications [38-41].
The SIW power dividers are one of recent technologies to overcome the previous disadvantages and combining advantages of both rectangular waveguides and Microstrip structures to achieve equal power division for multi wideband applications in the operating frequency range. There are several types as dividers: T, Y and Wilkinson power divider. The proposed structure in this paper is a new shape of the SIW three ports rhombic wraparound power divider where input power at port 1 is equally (-3 dB) transmitted to two isolated output ports 2 and 3.The SIW power dividers are essential component in different applications such as phased array, slot array , fractal array antenna and feeding systems which require split and dividing power equally over a wide bandwidth [42-45]. The proposed SIW divider introduces an equal and in-phase output power division from isolated ports 2 and 3. The proposed structure is shown in figure 6 and the main dimensions tabulated in table 5. The SIW divider is developed to obtain a wide bandwidth through inductive post in front of the input as a matched load stub. The inductive post reduces the reflection and splits the input power.

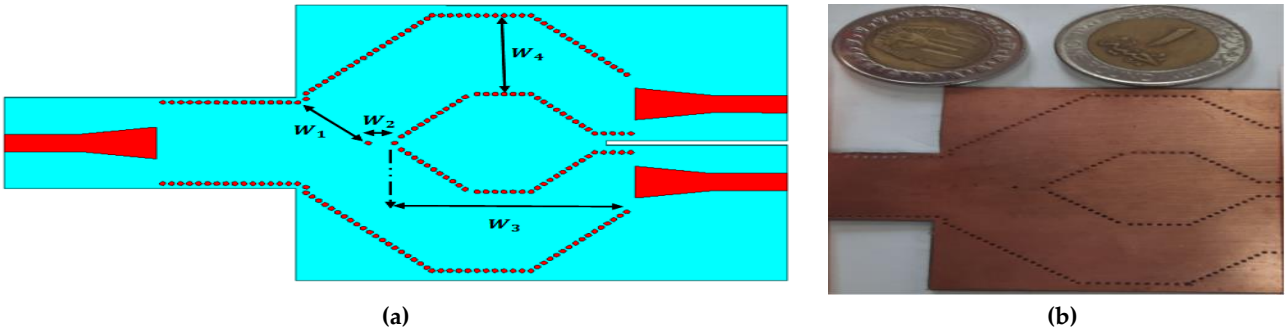

(a) (b)

Figure 6. The SIW rhombic wraparound divider: (a) The inner dimensions and view; (b) The implemented SIW divider.

Table 5. Dimensions of the SIW Rhombic Wraparound Divider/Combiner structure [mm].

Dimensions of the SIW Rhombic Wraparound Divider/Combiner Structure			
W_1	W_2	W_3	W_4
12.6	1.72	35.5	17.5

The SIW divider simulation results are shown in figure 7with the S-matrix extraction from HFSS simulator at 10.9 GHz as a minimum of $\boldsymbol{S_{11} = 0.03 S_{22} = 0.04 S_{33} = 0.05}$ in (12) from 6-13 GHz which introduces transmission coefficient $\boldsymbol{S_{12} = S_{13} = 0.64}$ as matching network connection. Also $\boldsymbol{S_{23} = S_{32} = 0.7}$as isolated output ports.

$$[S] = \begin{bmatrix} 0.03 & 0.64 & 0.64 \\ 0.64 & 0.04 & 0.7 \\ 0.64 & 0.7 & 0.05 \end{bmatrix} \quad (12)$$

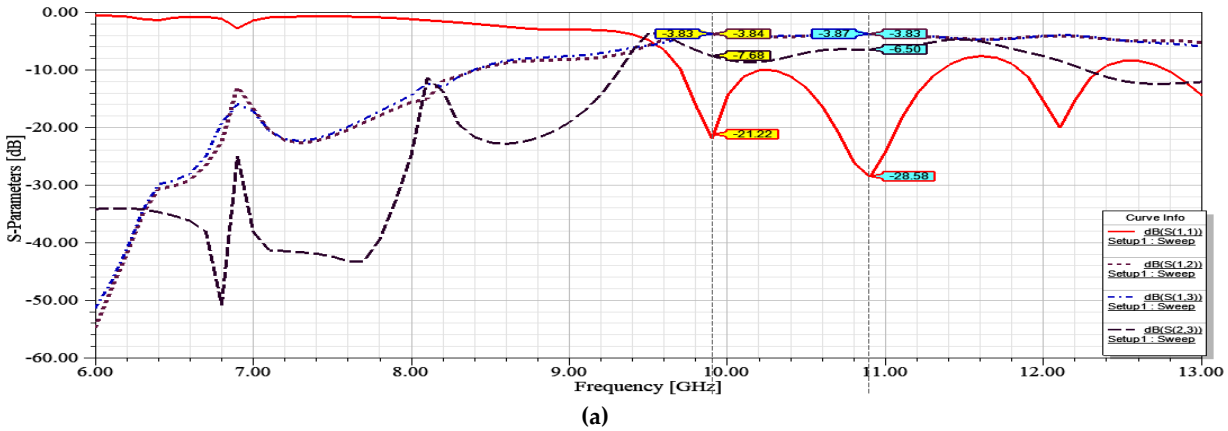

(a)

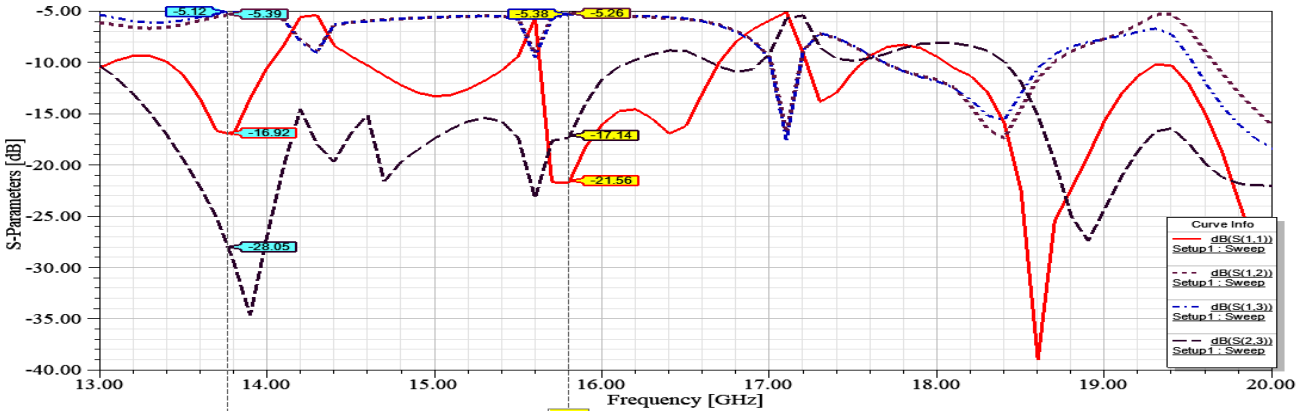

(b)

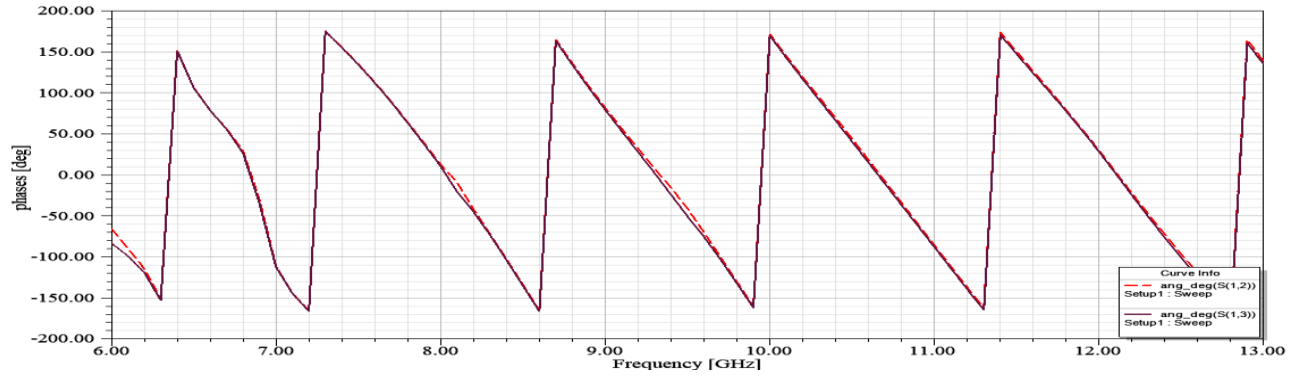

(c)

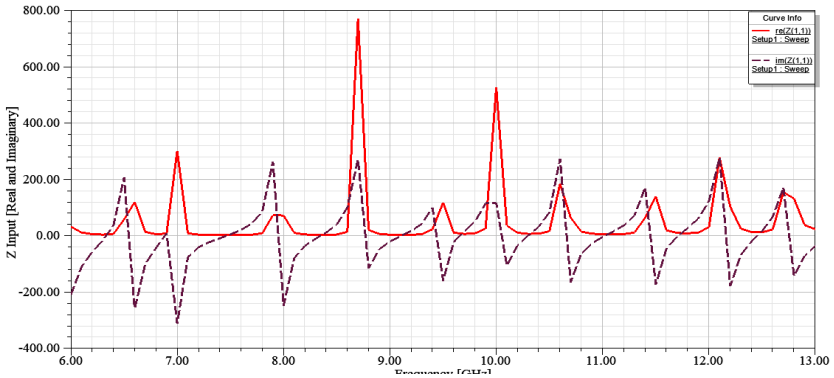

(d)

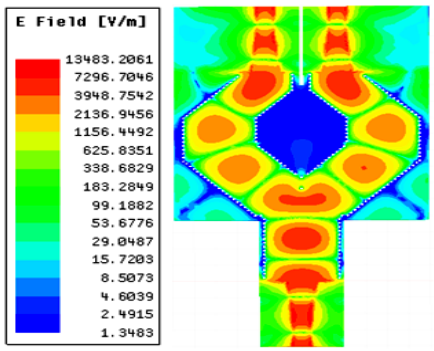

(e)

Figure 7. The SIW rhombic wraparound divider/combiner structure results: (a) The scattering parameters (1-13 GHz) [dB]; (b) The scattering parameters (13-20 GHz) [dB]; (c) The phase shift angle [deg.]; (d) The real and imaginary part of impedance [ohm]; (e) The electric field distribution [V/m].

Figures 7 (a and b) show the S-parameters for the proposed SIW divider from (6-13) GHz and (13-20) GHz respectively which confirms that the proposed divider is a multi-wide band in the operating frequency range. In X-Band two operating wide band has been obtained as (9.7-11.36) GHz and (11.84-12.35) GHz. Also in KU-Band three operating wide band has been obtained as (13.5-14.05) GHz, (14.55-15.46) GHz and (15.62-16.7) GHz. The multi wideband for the propose SIW divider are tabulated in table 6.From simulation results the output ports of the SIW divider have the same phase as shown in figure 7 (c) where they are isolated in transmission as shown figure 7 (a and b).Figure 7 (d and e) show the real and imaginary parts of the input impedance and the electric field distribution in [V/m] respectively which indicates that an excellent distribution of electric field through the SIW divider structure from input to output ports, is achieved.

Table 6. The SIW Divider Operating Bands.

Operating Bands of the SIW Divider/Combiner Structure [GHz]				
X-Band (8-12)		KU-Band (12-18)		
Band (1)	Band (2)	Band (1)	Band (2)	Band (3)
9.7-11.36	11.84-12.35	(13.5-14.05)	(14.55-15.46)	(15.62-16.7)

6. The SIW Slot Antenna

The SIW planar resonant slot antenna with shorted port for radar and satellite applications is proposed. Slots are located in the peak position of standing wave with slot separation of $\frac{\lambda_g}{2}$ for the same phase of all radiators. The shorted port is equivellent to open space where the last slot is $\frac{\lambda_g}{4}$ apart from this shorted port and the array is fed from the waveguide end. The equivalent circuit for such array is shown of figure 8 where the admittance Y is purely resistive with N slots in (13) [46-49].

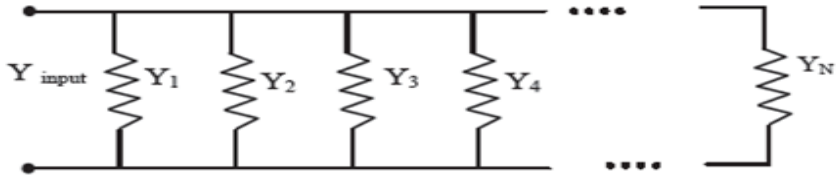

Figure 8. The schematic waveguide slot antenna equivalent circuit.

$$Y_{input} = Y_1 + Y_2 + Y_3 + Y_4 + Y_5 + \cdots \ldots \ldots + Y_N \tag{13}$$

Assume a resonant slot is in an infinitely conducting wall. The resonant slot length is assumed to be $\lambda_g/2$ in free space. If we use the normalized conductance, Gslot / Gwaveguide in (14) and (15), then we do not have to clutter the calculations with the waveguide conductance. Owing to the similarity between SIW and rectangular waveguides, most of H-plane waveguide components have been implemented in SIW [50-52].

$$\frac{g_{Slot}}{g_{Waveguide}} = g_1(\sin)^2\left(\frac{\pi x}{W}\right) \tag{14}$$

$$g_1 = \left(2.09\frac{W}{b}\frac{\lambda_g}{\lambda_0}\cos^2\left(\frac{\pi\lambda_0}{2\lambda_g}\right)\right) \tag{15}$$

where, W and b are the large and small dimensions of the waveguide, respectively,λ_0 is the free-space wave-length, x is the slot displacement from the waveguide centerline. The Conductance g is the real (resistive) part of admittance Y; if the slot is resonant, then the admittance has no reactive component.

In this section three varieties of SIW slot antenna have been designed, optimized using Rogger substrate and simulated using HFSS simulator for optimum design selection. Rectangular shape slot, rotated rectangular shape slot and a hybrid of both rectangular and rotated construct the lamda shape slot are the three varieties respectively. Figure 9 shows the proposed varieties, and the main dimensions are tabulated in table 7.

Table 7. Dimensions of the SIW Slot Antenna Varieties [mm].

Dimensions of the SIW Rectangular Shape Slot Antenna Structure								
L_{SL}	W_{sL}	W_{S1}	L_{RS}	W_{RS1}	D_{w4}	Angle α [Degree]	$L_{S1} = \lambda_g/4$	$L_{S2} = \lambda_g/2$
11.2	0.5	6.25	5.75	5.1	1	22.5	7.25	14.5

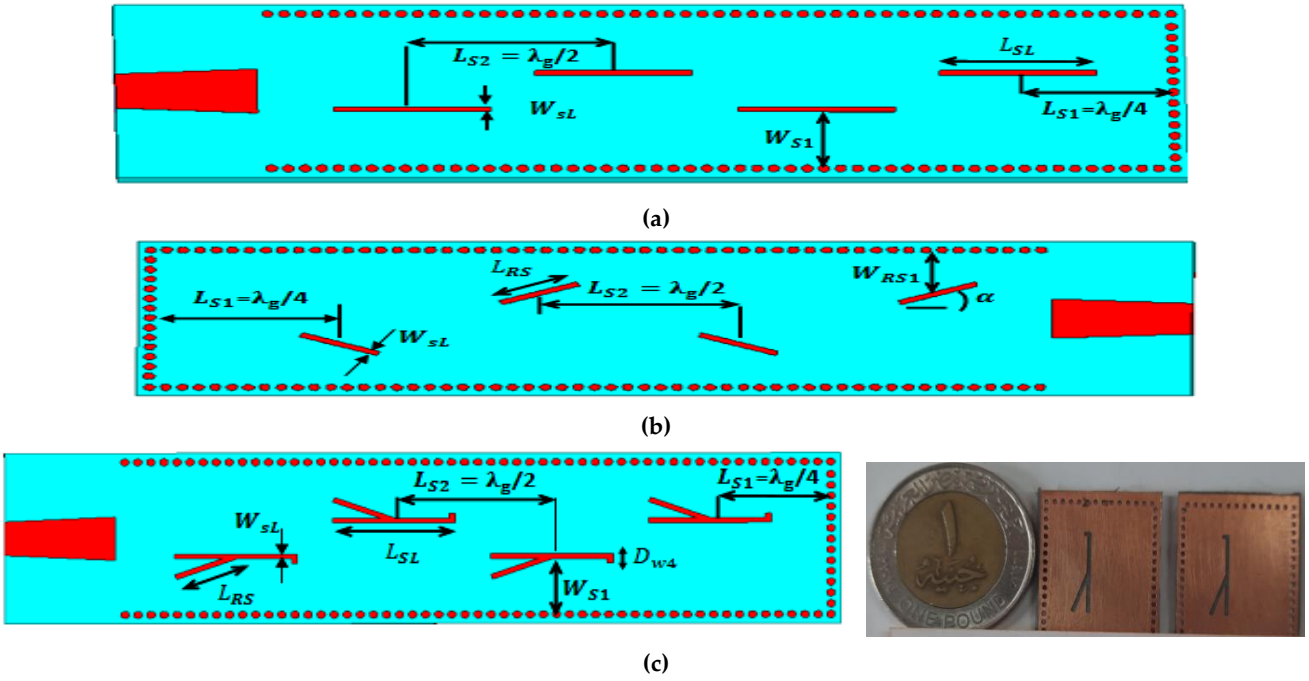

Figure 9. The SIW slot antenna varieties: (a) Rectangular shape slot; (b) Rotated rectangular shape slot; (c) Lamda shape slot and implemented structure.

The return loss simulation results for the proposed three varieties are shown in figure 10 which show that the optimum selection is the lamda shape slot antenna as the improvement of $\mathbf{S_{11} = -25.53\ dB}$, maximum absolute gain = 9 and 98% radiation efficiency for 1 W incident power. All parameters for the proposed varieties and selected one are shown in table 8. The radiation efficiency is calculated as: (Radiated power/accepted power)×100.

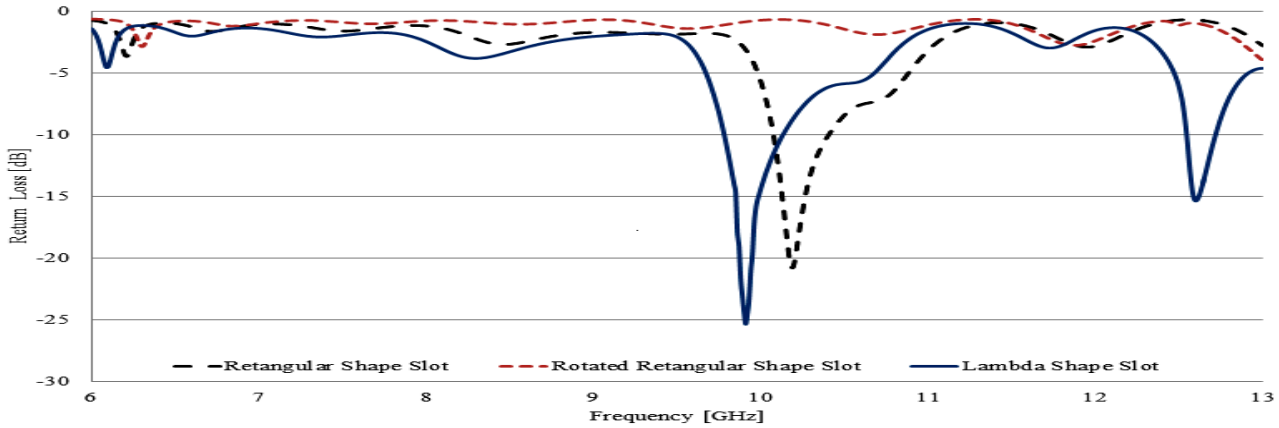

Figure 10. The return loss comparison of the SIW slot antenna varieties [dB].

Table 8. The SIW Slot Antenna Parameters for the Three Varieties.

The SIW Slot Antenna Parameters for the Three Varieties Respectively									
Slot Varity	Freq. [GHz]	Return Loss [dB]	Max.U [W/Str.]	Incident Power [W]	Accepted Power [W]	Radiated Power [W]	Gain [Abs.]	Directivity [Abs.]	Radiation Efficiency [%]
1	10.19	-20.73	0.629	1	0.991	0.948	7.972	8.338	96
2	11.85	-2.7	0.094		0.465	0.402	2.55	2.945	87
3	9.91	-25.53	0.72		0.992	0.981	9.016	9.2	98

Simulation results such as gain, directivity, radiation pattern and surface current distribution on the surface of antennas for the three varieties are shown in Figures 11, 12 and 13 for the proposed structures respectively.

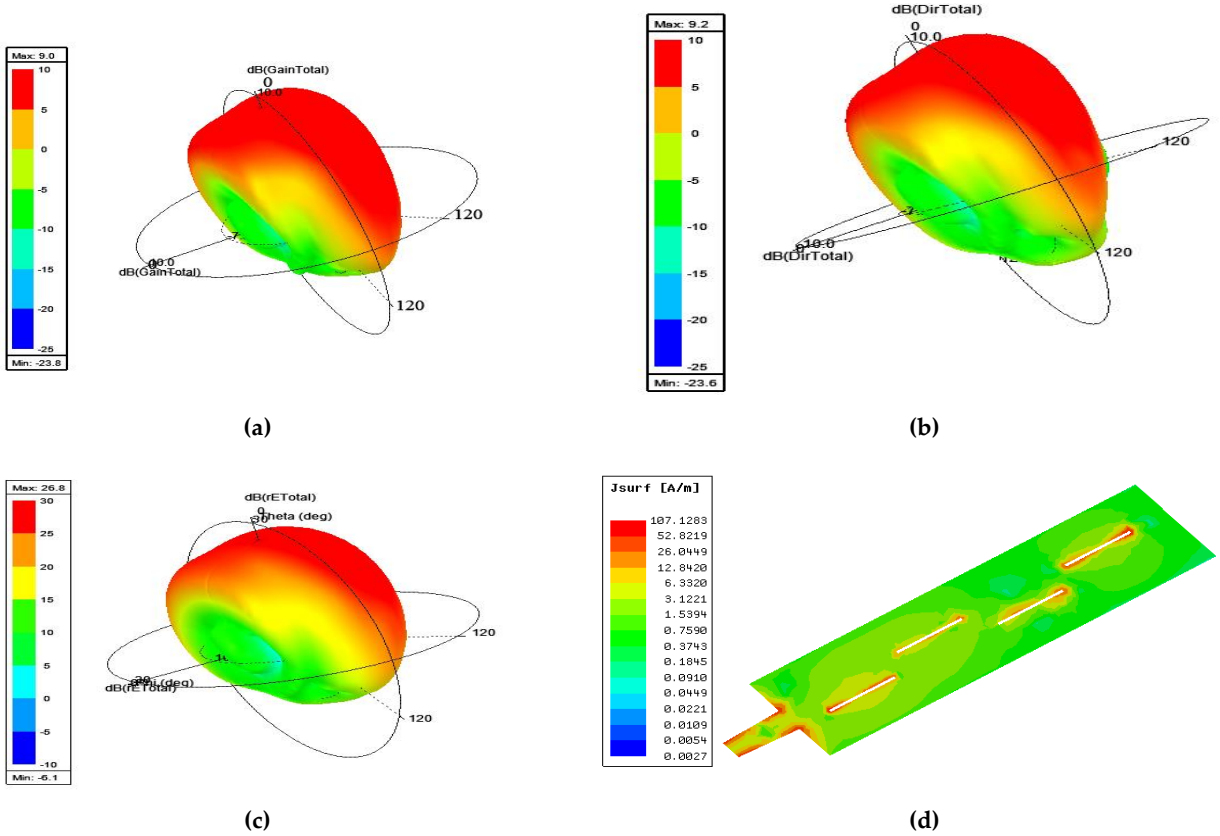

Figure 11. The SIW rectangular shape slot antenna structure simulation results:(a) The 3 D antenna gain [dB]; (b) The 3 D antenna directivity [dB]]; (c) The 3 D antenna radiation pattern; (d) The surface current distribution [A/m].

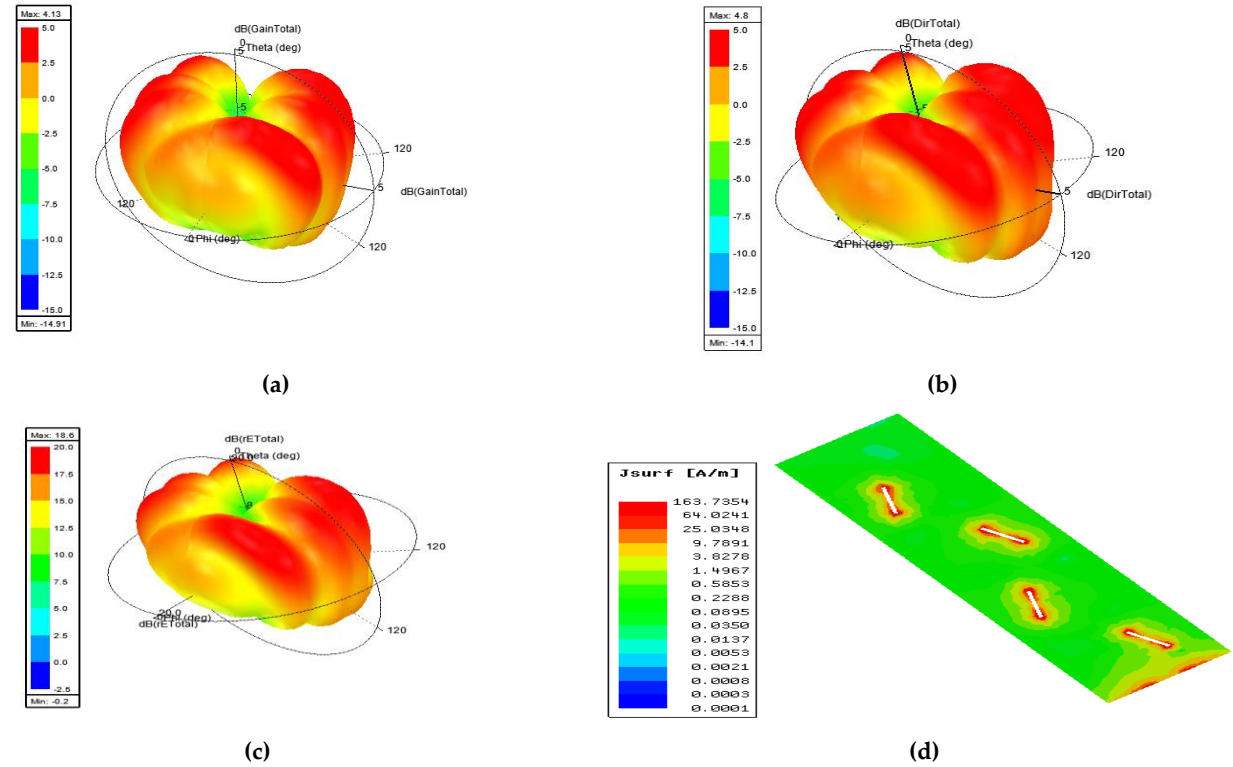

Figure 12. The SIW rotated rectangular shape slot antenna structure simulation results: (a) The 3 D antenna gain [dB]; (b) The 3 D antenna directivity [dB]]; (c) The 3 D antenna radiation pattern; (d) The surface current distribution [A/m].

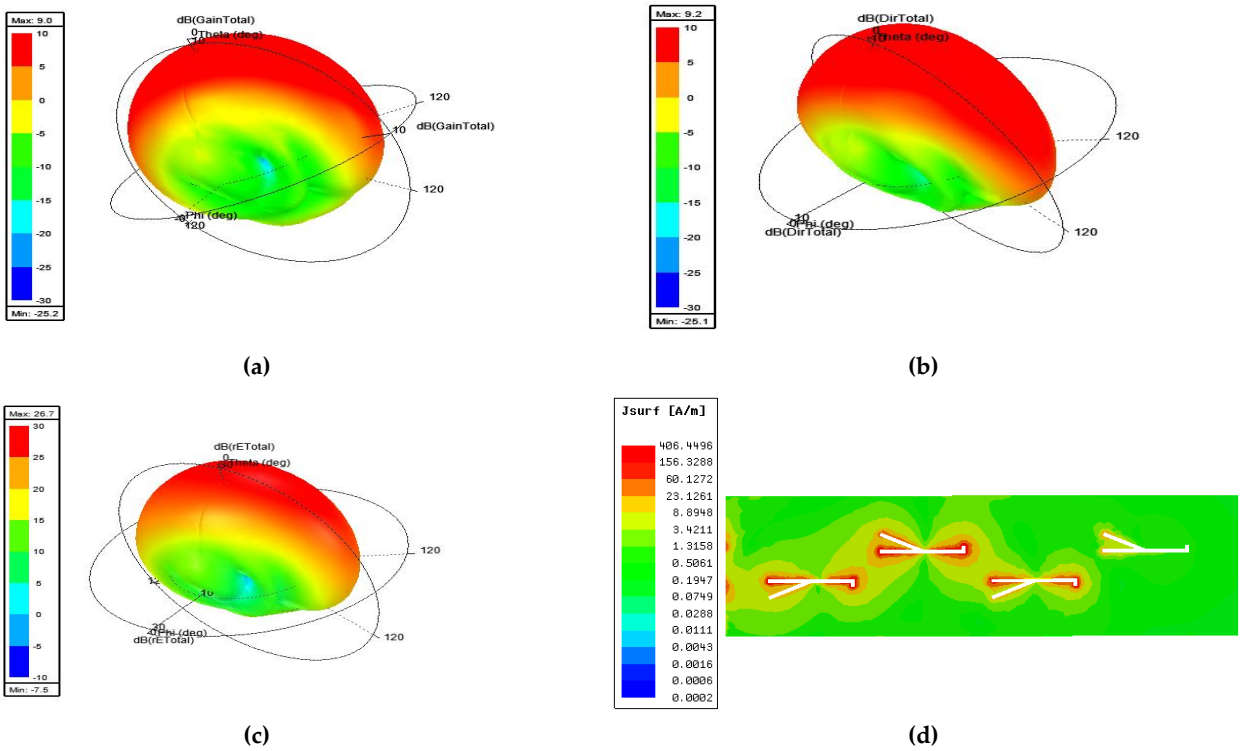

Figure 13. The SIW lamda shape slot antenna structure simulation results: (a) The 3D antenna gain [dB]; (b) The 3 D antenna directivity [dB]]; (c) The 3D antenna radiation pattern; (d) The surface current distribution [A/m].

From simulation results in figures 11, 12 and 13 we conclude that the lamda shape slot which is a hybrid connection of the designed rectangular slot has an acceptable and optimum current distribution all over the whole surface of the structure for optimum performance of the structure as shown in figure 13 (d) which will be used in fractal antenna implementation.

7. The SIW Hexagonal Diamond of Lamda Shape Slots Fractal Array Antenna

In the field of fractal antenna engineering the fractal, means broken or irregular fragments, to describe a complex shape that possess an inherent self-similarity in their structure. Object which has a very small or fractional size and dimensions is a recursively generated and called a fractal object. The recursive natural of fractal is used to design different varieties of antenna objects [53-58]. Fractal array antennas have many important properties such the independence of frequency, multi band characteristics, low side lobe and the ability of development of beam forming algorithms fractal structures. Fractal array antennas can be formed recursively by the repetitive of generating sub-array to construct the full array structure [59-64]. The sub-array elements are turned off and on in a specific pattern. Hence the fractal arrays is composed of the sequential of the self-similar sub-arrays. Different shapes of fractal array antennas exist: such Minkowshi island, Koch loop, plant fractals in nature, Pascal's triangle, circular and Koch loops, Sierpinski carpet arrays, Sierpinski gasket array and hexagonal array.

In this section three varieties of SIW slot fractal antenna based on using selected lamda shape slot has been introduced, designed, optimized, and analyzed for optimum design to be integrated with both divider and phase shifter. The three varieties are the first stage of the hexagonal fractal antenna constructed of three lamda slot elements. The second stage of the proposed hexagonal is constructed of six groups of the one stage with total 18 elements of lamda shape slot repeated twice in the SIW structure. The final hexagonal structure is the three stages which consist of seven groups of the second stage with total of 126 elements of lamda shape slot. The final structure of the proposed hexagonal fractal array will be integrated with other system previous components for the proposed application. Figure 14 shows the fractal antenna varieties, and the main dimensions are tabulated in Table 9 and the comparison simulation results shown in Figure 15.

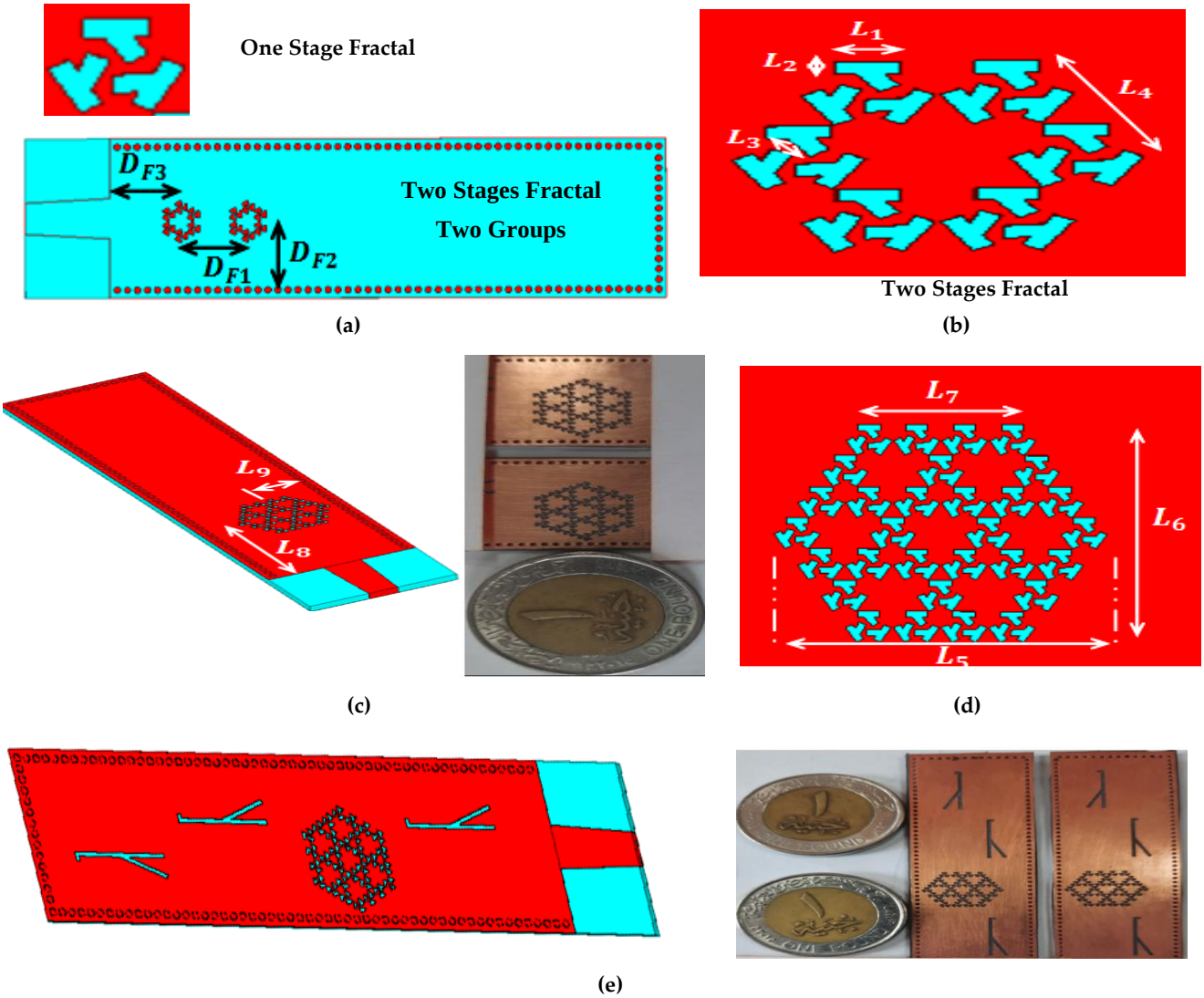

Figure 14. Stages of SIW hexagonal fractal antenna structure with implemented view: (a and b)One and Two stages;(c and d)Three stages; (e) The final stage Hybrid Fractal and Lamda structure .

Table 9. Dimensions of Stages of SIW Hexagonal Shape Antenna Structure [mm].

Dimensions of Stages of SIW Hexagonal Shape Antenna Structure											
L_1	L_2	L_3	L_4	D_{F1}	D_{F2}	D_{F3}	L_5	L_6	L_7	L_8	L_9
0.8	0.3	0.5	2.5	8	8.1	8.5	5.9	11.4	11.85	18	6.5

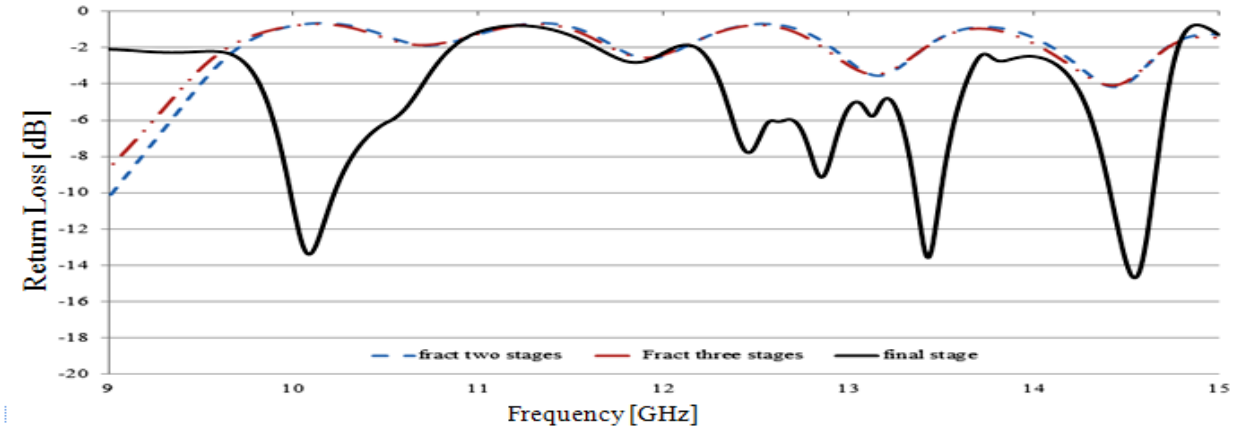

(a)

Figure 15. The SIW hexagonal diamond of lamda shape slot varieties fractal array antenna simulation results.

From simulation results shown in figure 15, it is clear to notice that the final structure of the proposed hexagonal shape of lamda slot elements has a minimum reflection of about -14 dB, -14.2 dB and -14.5 at (10.1, 13.6 and 14.6) GHz for impedance matching network at these frequencies. Simulation results for stages such as gain, directivity, radiation pattern and surface current distribution are shown in Figures 16 and 17.

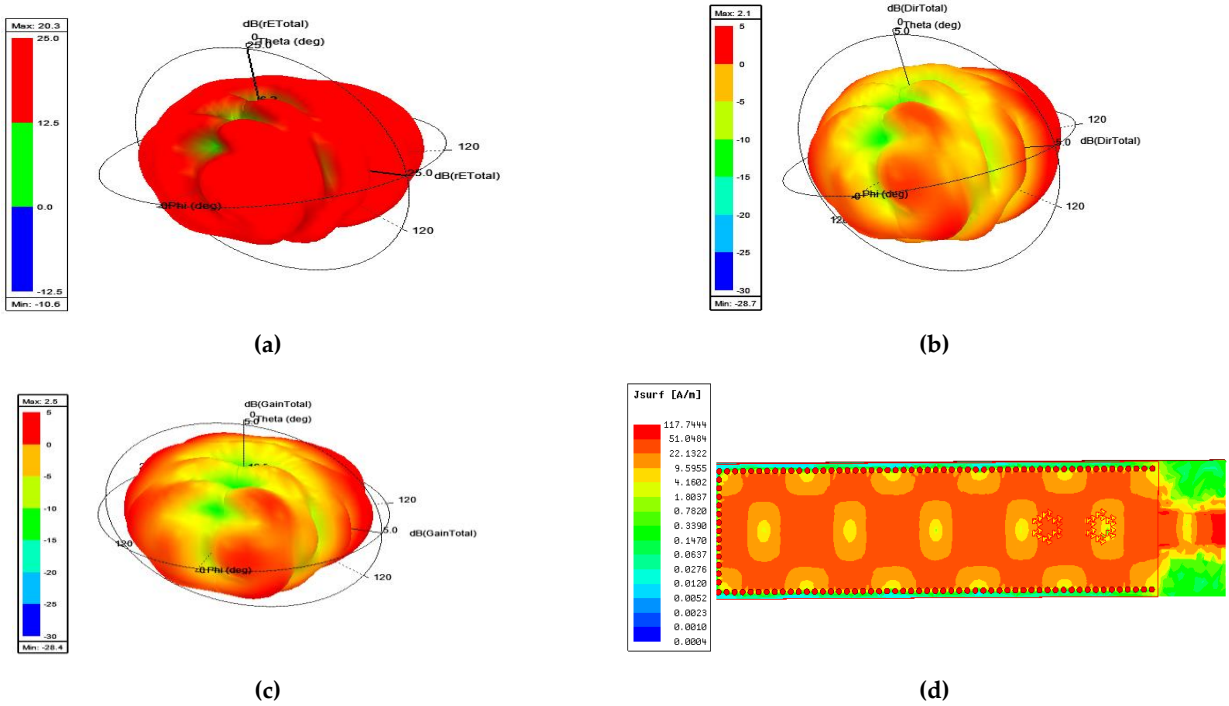

(a) **(b)**

(c) **(d)**

Figure 16. The two stages of SIW hexagonal shape antenna structure simulation results:(a) The 3D antenna gain [dB]; (b) The 3D antenna directivity [dB]]; (c) The 3D antenna radiation pattern; (d) The surface current distribution [A/m].

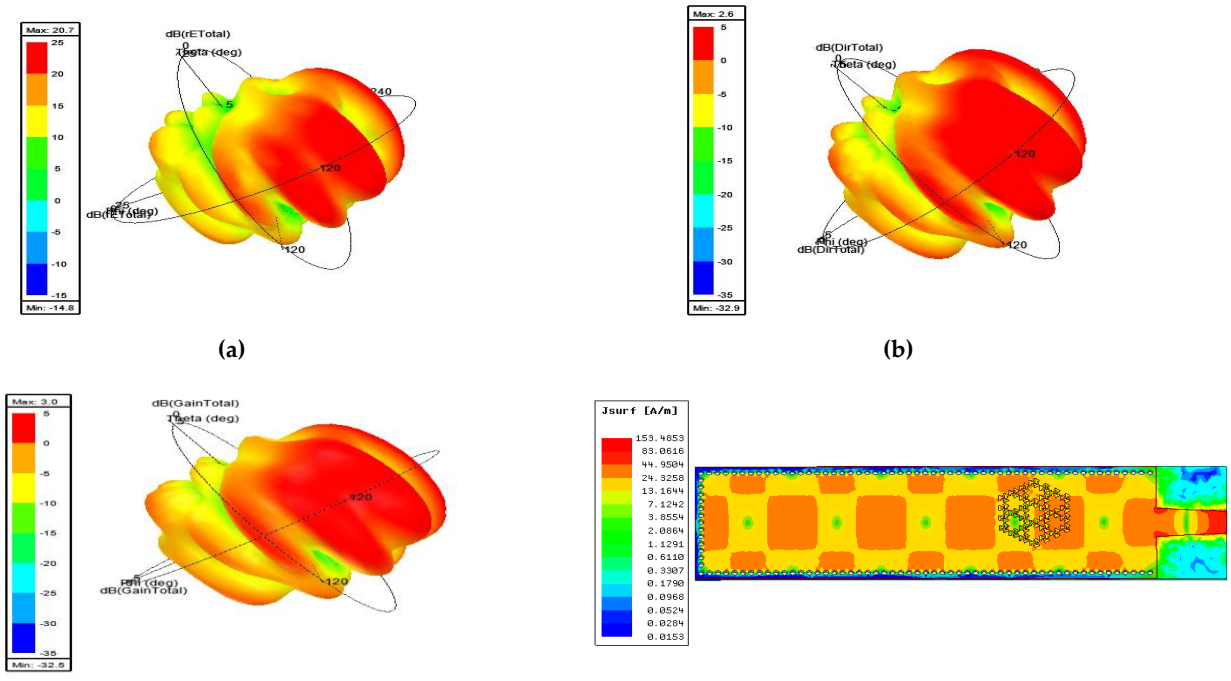

(a) **(b)**

(c) **(d)**

Figure 17. Three stages of SIW hexagonal shape antenna structure simulation results: :(a) The 3Dantenna gain [dB]; (b) The 3D antenna directivity [dB]]; (c) The 3Dantenna radiation pattern; (d) The surface current distribution [A/m].

The fractal arrays can be formed recursively through the repetition of sub-array. A sub-array is a small structure at scale one (P = 1) used to **con**struct the full one (P > 1).A set formula is needed for scaling and translation of the sub-array in order to produce the fractal array. The array factor for a fractal array is expressed as in (16) [53-55],where $GA(\psi)$is the array factor sub-array,$\delta$is a scale or expansion factorthat governs how large the array grows with each recursive applicationof the generating sub array especially in radar applications [65].

$$\mathrm{AF_P}(\psi) = \prod_{\mathrm{P=1}}^{\mathrm{P}} \mathrm{GA}(\delta^{\mathrm{P-1}}\psi) \tag{16}$$

Hexagonal structures are planar array configuration and have important applications in wireless communications. The hexagonal array structure constructed by placing a single element, surrounded by several six elements formed Hexagonal shape array. The array factor with six-element sub-array can be represented as in (17), where $\emptyset_n = (n-1)\frac{\pi}{3}$ and $\alpha_n = -\pi sin\theta_0 cos(\emptyset_0 - \emptyset_n)$.

$$\widehat{\mathrm{AF}}_{\mathrm{P}}(\theta,\emptyset) = \frac{1}{6^{\mathrm{P}}}\prod_{\mathrm{P=1}}^{\mathrm{P}}\sum_{\mathrm{n=1}}^{6} \mathrm{e}^{\mathrm{j}\delta\mathrm{p}-1}[\pi\mathrm{sin}\theta\mathrm{cos}(\phi-\phi_{\mathrm{n}})+\alpha_{\mathrm{n}}] \tag{17}$$

$$\widehat{\mathrm{AF}}_{\mathrm{P}}(\theta,\emptyset) = \frac{1}{6^{\mathrm{P}}}\prod_{\mathrm{P=1}}^{\mathrm{P}}\sum_{\mathrm{n=1}}^{6} \mathrm{e}^{\mathrm{j}\delta\mathrm{p}-1}\,\psi_{\mathrm{n}}(\theta,\emptyset) \tag{18}$$

$$\psi_{\mathrm{n}}(\theta,\emptyset) = \pi[\mathrm{sin}\theta\mathrm{cos}(\phi-\phi_{\mathrm{n}}) - \mathrm{sin}\theta_0\mathrm{cos}(\phi_0-\phi_{\mathrm{n}})] \tag{19}$$

For the unity of the recursive hexagonal array d to be unity ($\delta = 1$), we obtain (20) and these arrays increase in size at a rate that obeys the relationship in (21), Where $\delta_{\mathrm{p1}}$is the Kronecker delta function defined by (22).

$$\widehat{\mathrm{AF}}_{\mathrm{P}}(\theta,\emptyset) = \left[\frac{1}{6}\sum_{\mathrm{n=1}}^{6} \mathrm{e}^{\mathrm{j}\psi_{\mathrm{n}}(\theta,\emptyset)}\right]^{\mathrm{P}} \tag{20}$$

$$\mathrm{N_P} = 3\mathrm{P}(\mathrm{P}+1) + (1-\delta_{\mathrm{P1}}) \tag{21}$$

$$\delta_{\mathrm{p1}} = \begin{cases} 1, & \mathrm{p} = 1 \\ 0, & \mathrm{p} \neq 1 \end{cases} \tag{22}$$

This means that, the number of concentric hexagonal sub-arrays contained in it increases by one for every time this fractal array evolves from one stage to the next. Figure 18 shows simulation results for the final hexagonal shape fractal array antenna. Simulation results introduce return loss, VSWR, input impedance, gain, directivity radiation pattern and surface current distribution on the structure.

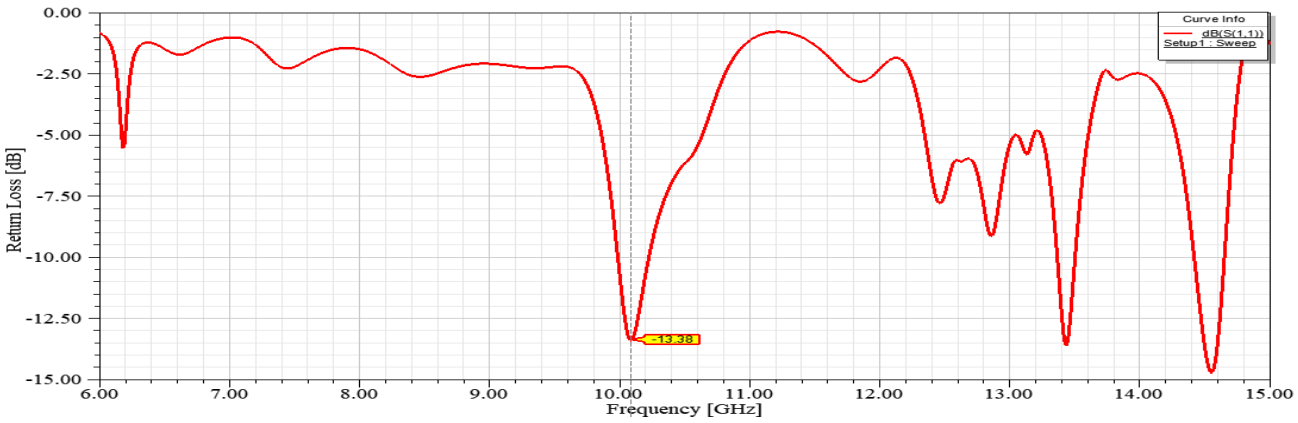

(a)

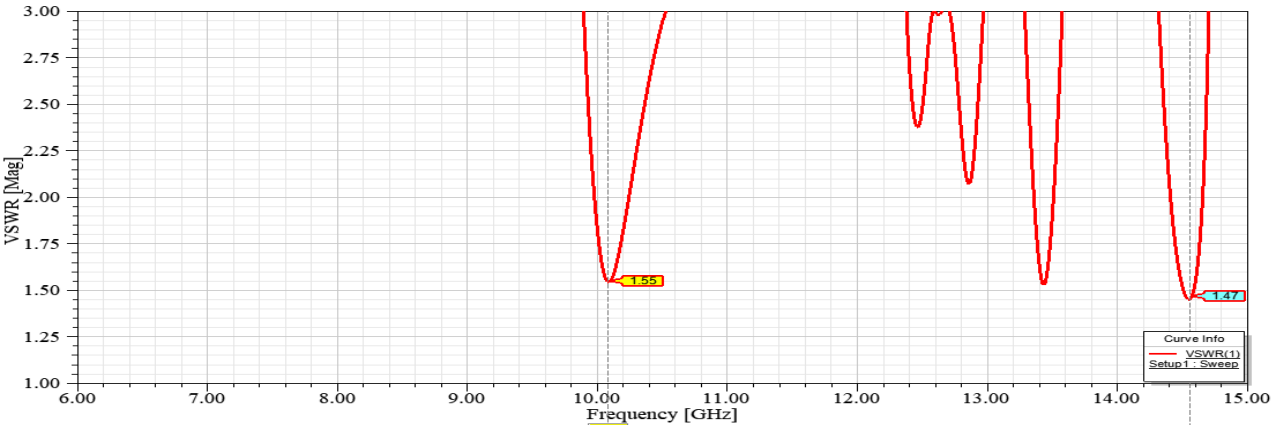

(b)

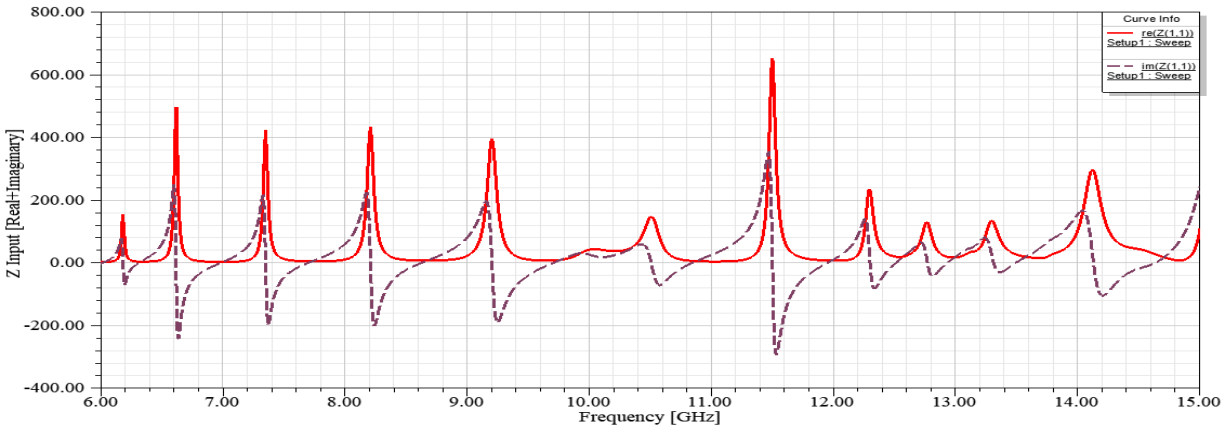

(c)

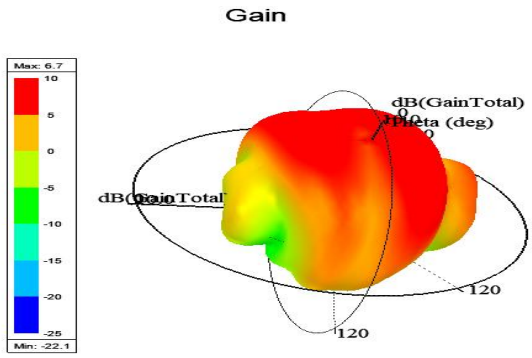

(d)

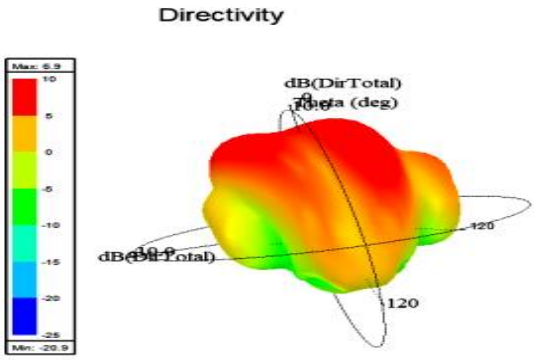

(e)

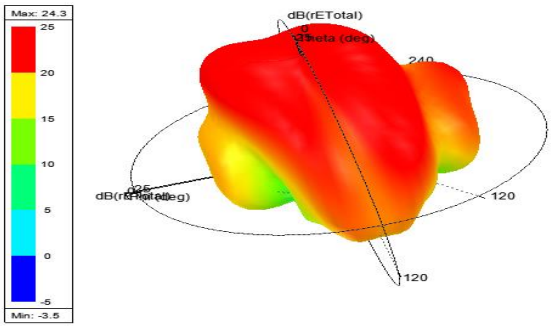

(f)

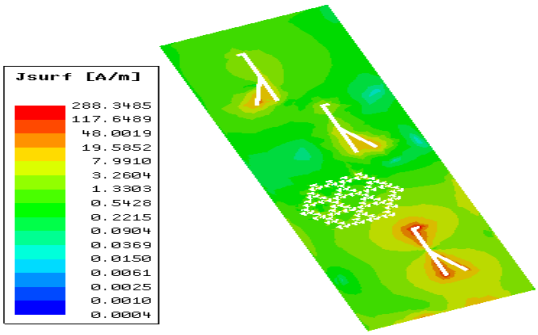

(g)

Figure 18. The SIW hexagonal diamond array with three elements of Lamda shape simulation results: (a) The return loss [dB]; (b) The VSWR; (c) The input impedance [Ω]; (d) The 3 D polar plot antenna gain [dB]; (e) The 3 D polar plot antenna directivity [dB]; (f) The 3D radiation pattern; (g) The surface current distribution [A/m].

Table 10. The Final SIW, Hybrid of Hexagonal Diamond and Lamda Array Antenna Parameters.

The SIW,Hybrid of Hexagonal Diamond and Lamda Array Antenna Parameters								
Freq. [GHz]	Return Loss [dB]	Max.U [W/Str.]	Incident Power [W]	Accepted Power [W]	Radiated Power [W]	Gain [Abs.]	Directivity [Abs.]	Radiation Efficiency [%]
10.08	-13.38	0.357	1	0.95	0.9	4.7	4.98	95

Table 10 gives summarized of the final SIW, hybrid of hexagonal and lamda array antenna parameter which gives a good performance with reflection coefficient reaching to -13.38 dB as a matching parameter and maximum absolute gain of 4.7 with 95 % radiation efficiency. All other parameter illustrated in the given table.

8. The Full Integrated SIW System Simulation and Implementation Results

This section is divided into three subsections, the subsection 8.1 introduces the structure, simulation results and antenna parameters for the final integrated system which is a compact in size compared with similar SIW technologies [66], the subsection 8.2 presents implementation results of the same full system. Finally in the subsection 8.3 a comparison between simulation and implementation results have been presented to confirm the agreement between both results over most of frequency range.

8.1 The Full Integrated SIW System Simulation Results

The proposed full SIW integrated system structure which consists of the basic SIW with tapering transition structure, the SIW rhombic divider/combiner, the SIW phase shifter and two arrays of the final SIW hybrid of hexagonal diamond and lamda array on the two output ports with phase shifter in one of them is shown in figure 19. Simulation results for the full integrated system and its antenna parameters for about eleven operating frequencies have been presented from (5-18) GHz in figure 20 and tables 11 respectively. Comparing these results with slot SIW slot antenna in [51] indicates that the proposed antenna has more enhancements in antenna parameters such as the return loss in [51] reaches -20 dB compared with -43 dB in the proposed structure in addition to the multiple operating frequency.

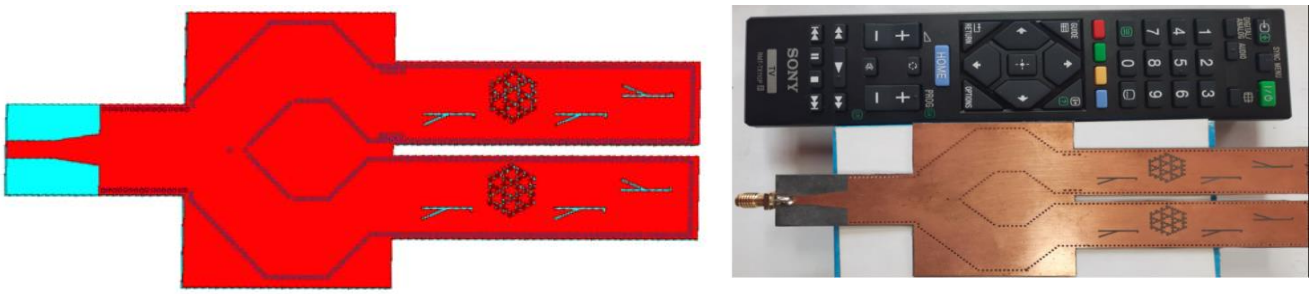

Figure 19. The full integrated SIW system.

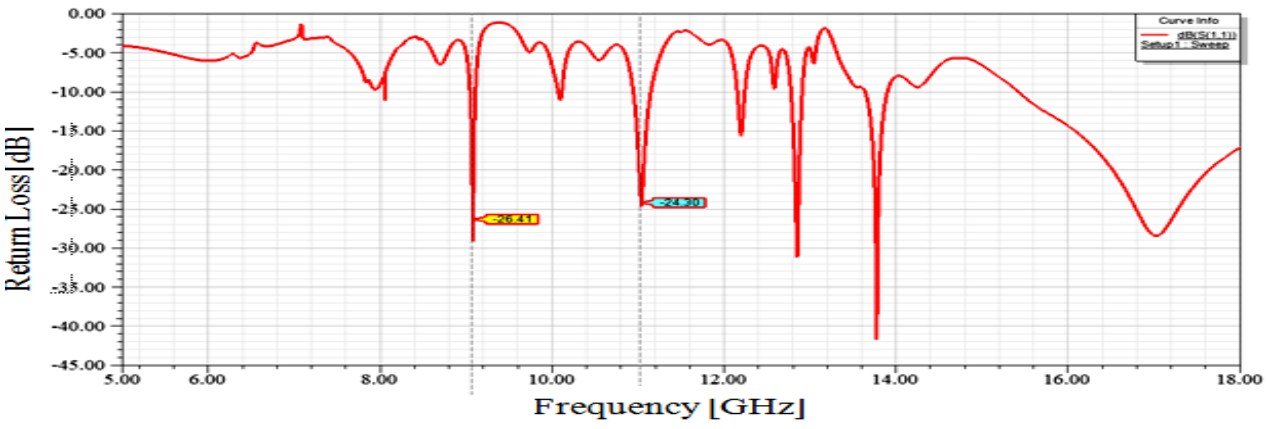

(a)

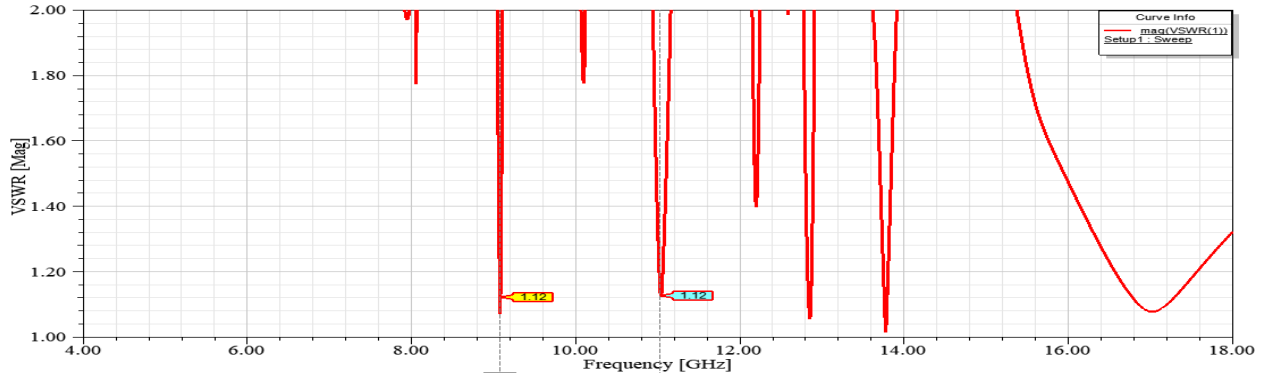

(b)

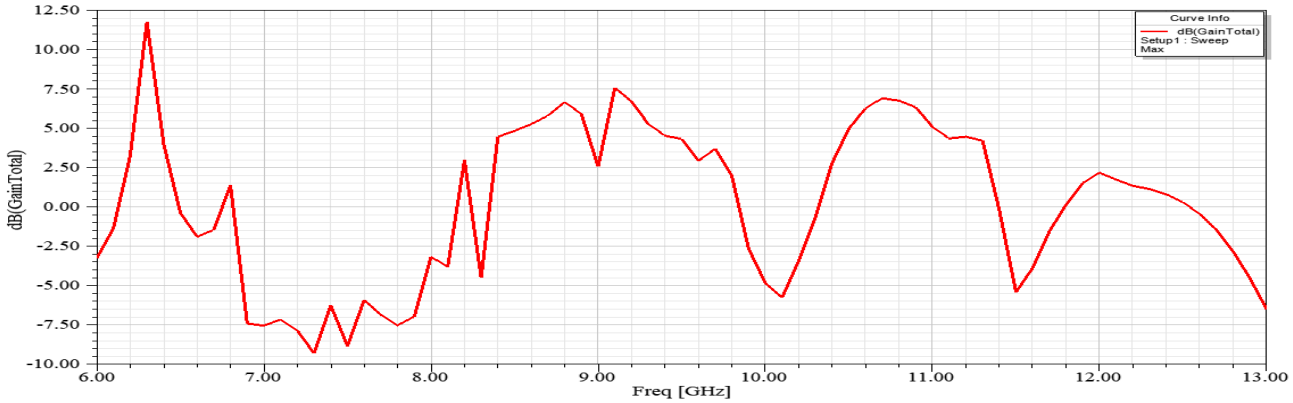

(c)

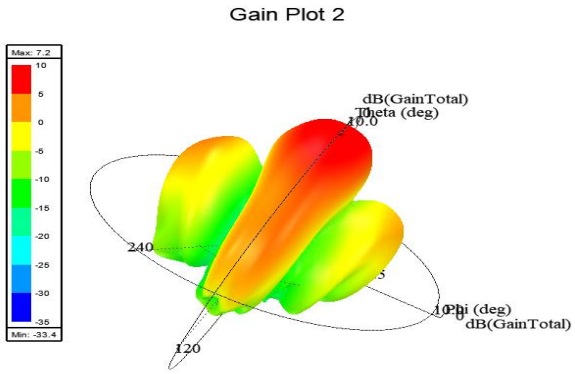

(d)

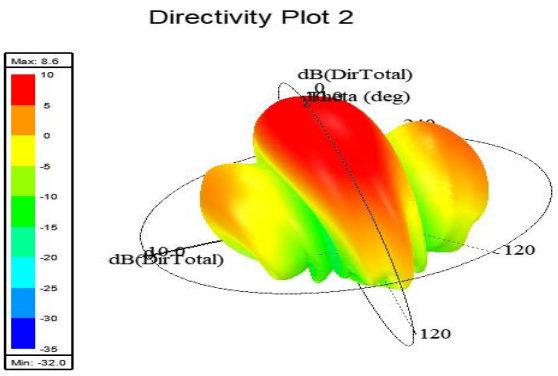

(e)

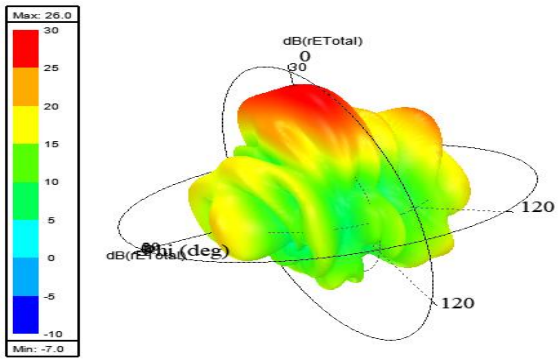

(f)

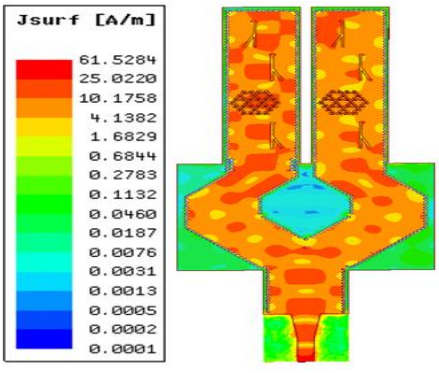

(g)

Figure 20. The full integrated SIW system simulation results: (a) The return loss [dB]; (b) The VSWR; (c)The gain verses frequency[dB]; (d) The 3 D antenna gain [dB]; (e) The 3 D antenna directivity [dB]; (f) The 3D radiation pattern; (g) The surface current distribution [A/m].

Table 11. The Full Integrated SIW System Antenna Simulated Parameters at Different Improved Return Loss Frequencies.

The Full Integrated SIW Antenna Parameters								
Freq. [GHz]	Return Loss [dB]	Max.U [W/Str.]	Incident Power [W]	Accepted Power [W]	Radiated Power [W]	Gain [Abs.]	Directivity [Abs.]	Radiation Efficiency [%]
7.94	-10	0.0173		0.893	0.198	0.243	1.099	22
9.071	-29.8	0.477		0.996	0.633	6.012	9.449	63
10.093	-10.2	0.361		0.921	0.876	4.918	6.563	95
10.096	-10.3	0.361		0.921	0.885	4.914	6.557	96
11.034	-25	0.545		0.997	0.859	6.878	7.981	86
12.183	-15	0.369	1	0.969	0.708	4.798	6.562	73
12.878	-16	0.338		0.978	0.704	4.347	6.041	72
13.764	-32	0.642		0.999	0.895	4.914	6.545	96
13.769	-43	0.724		0.999	0.985	7.1	9.7	97
16.112	-15	0.136		0.971	0.623	1.760	8.246	64
17.087	-30	0.121		0.998	0.742	1.519	9.439	74

8.2 The Full Integrated SIW System Implementation Results

The designed, analyzed and simulated full SIW system in subsection 8.1 have been implemented using Rogger RT/duriod 5880 substrate of $\varepsilon_r = 2.2$, $\tan\delta = 0.0009$ and $h_R = 0.79$ mm and its measured results will be introduced in this section. The full SIW system has been tested in laboratory using (R&S ZVB 20 VECTOR NETWORK ANALYZER 10-20 GHz). The measurement connection and its measured results from (5-18) GHz for both X and KU-Bands applications are illustrated in Figures 21 and 22.

Measured results illustrated in Figure 23 introduce more than 20 frequency of return loss less than -10 dB and are tabulated in Table 12 as operating frequencies with minimum return loss and hence more effective in radiating power for the proposed structure.

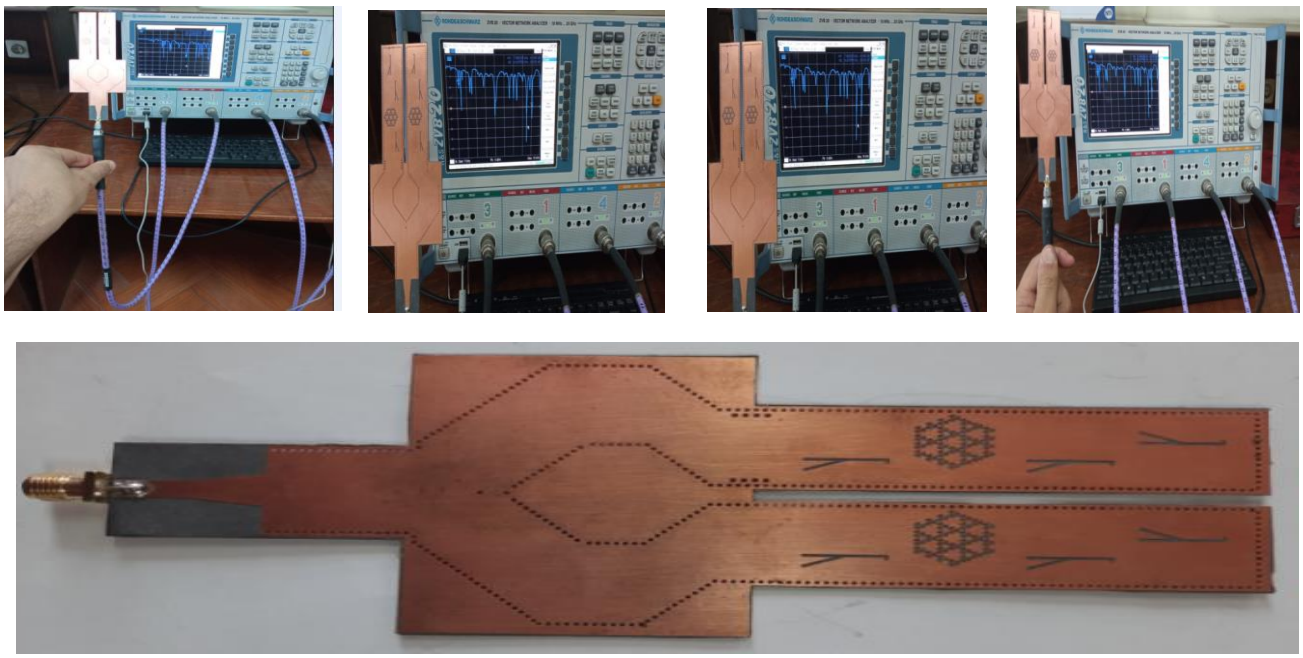

Figure 21. The full integrated SIW implemented system measurement connection.

Table 12. The Full Integrated SIW System Antenna Measured Parameters at Different Improved Return Loss Frequencies.

Freq. [GHz]	Return Loss [dB]	Freq. [GHz]	Return Loss [dB]	Freq. [GHz]	Return Loss [dB]	Freq. [GHz]	Return Loss [dB]	Freq. [GHz]	Return Loss [dB]
7.98	-10	10	-10	12.8	-16	14.3	-24	15.7	-16
8.14	-23	10.9	-24	13.7	-34	1`4.9	-12	16.2	-48
8.9	-12	12.2	-15	14	-25	15.5	-24	16.9	-33
9	-13	12.6	-15.3	14.2	-24	15.6	-17	17	-24

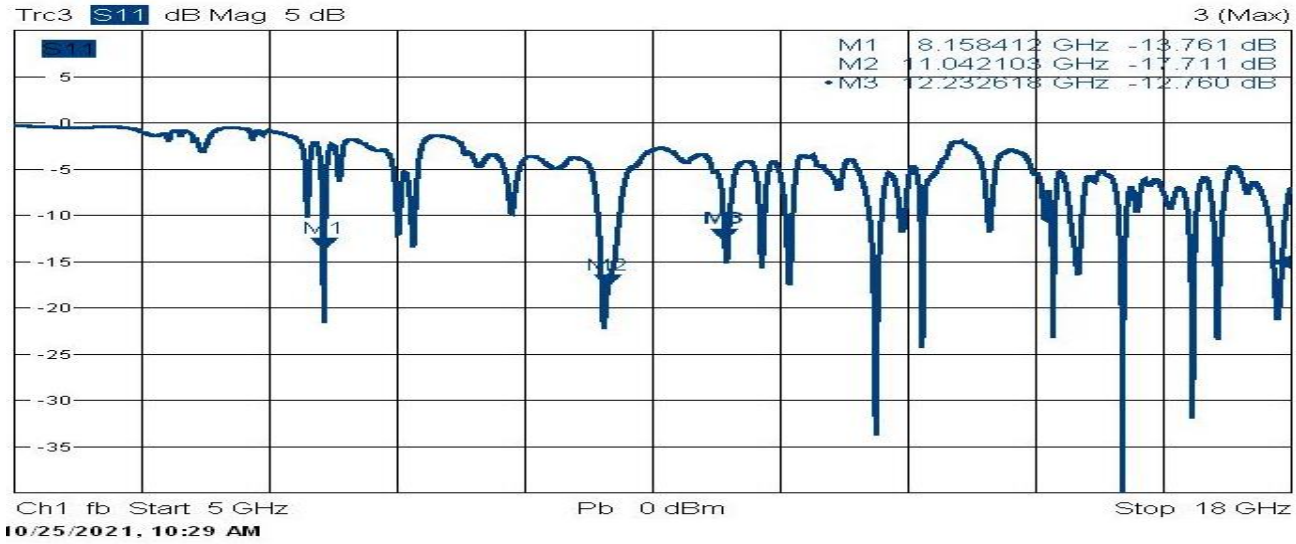

Figure 22. The full integrated SIW implemented system measured results.

8.3 The Full Integrated SIW System Simulation and Implementation Results

Comparison between simulated and measured results for the full integrated SIW system is introduced in this subsection to indicate how both results agree and to confirm the presented analysis for all designed and simulated structures in this paper. Figure 23 shows the comparison results.

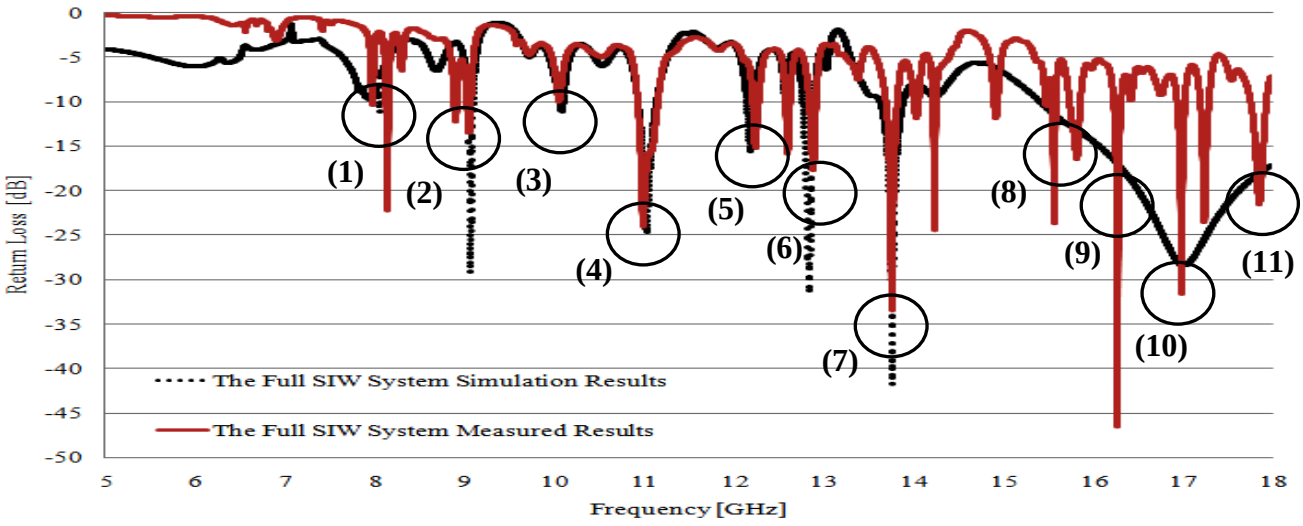

Figure 23. Comparison between simulated and measured results for the full integrated SIW system.

As a conclusion, Figure 23 shows the agreement and closed results between simulated and measured results for about eleven operating frequencies over the frequency band from (5-18) GHz for both X and KU-Bands applications. The proposed design has cutoff frequency equals 6.15 GHz for the dominant mode and the operating

frequency must be greater than this cutoff frequency. The start of operating frequency for the proposed structure is 8 GHz and below this value there is a less agreement between simulation and measured results. The agreement between simulation and implementation results is from 8 GHz to 15 GHz and however due the numerical calculation and mesh dividing of the software which depend on the FEM there is less agreement between simulation and measured results above 15 GHz.

9. Conclusions

Fractals play vital role to reduce the size of switchable fractal antenna with optimized gain and other antenna parameters. With the increase of the iterations of fractal the resonant frequency increases with minimal return loss. Fractal geometry enables us to obtain the multiband wideband characteristics. These characteristics are used for different applications such, military and wireless communication. The SIW integrated system introduces multiple operating frequencies in both X and Ku-Bands. Agreement and close of about 11 resonance operating frequency of the radiating antenna for both simulated and measured results are shown in figure 23 with minimum return loss of -43 dB, maximum absolute gain 7.1 with 98 % radiation efficiency. The integrated SIW system meets the requirement of radar application in the proposed operating frequency range.

References

1. Nantista, C. Overmoded rectangular waveguide components for a multi-moded RF power distribution system (No. SLAC-PUB-8500).Stanford Linear Accelerator Center, Menlo Park, CA (US).2000
2. Martyniuk, S. Y., Dubrovka, F. F., Zakharchenko, O. S., & Stepanenko, P. YEffective High-Precision Analysis of Thin Asymmetric Inductive Diaphragm in Rectangular Waveguide Using Integral Equation Method. Radioelectronics and Communications Systems, 2021, 64(2), 80-91.
3. Shah, A., & Patel, P. Broadband coplanar waveguide-fed stub loaded pot shape E-textile antenna equipped with perfect electric conductor. International Journal of RF and Microwave Computer-Aided Engineering, 2021, 31(5).
4. Abdelaziz, A., &Hamad, E. K. Design of a compact high gain microstrip patch antenna for tri-band 5 G wireless communication. Frequenz, 2019, 73(1-2), 45-52.
5. Feng, S., Zhang, L., Yu, H. W., Zhang, Y. X., & Jiao, Y. C. A single-layer wideband differential-fed microstrip patch antenna with complementary split-ring resonators loaded. IEEE, 2019.
6. Mathur, P., & Kumar, G. Dual frequency dual polarized shared-aperture microstrip antenna array with suppressed higher order modes. IET Microwaves, Antennas & Propagation, 2019, 13(9).
7. Shi, J., Zhu, L., Liu, N. W., & Wu, W. A microstrip Yagi antenna with an enlarged beam tilt angle via a slot-loaded patch reflector and pin-loaded patch directors. IEEE Antennas and Wireless Propagation Letters, 2019, 18(4), 679-683.
8. Hong, W., Liu, B., Wang, Y., Lai, Q., Tang, H., Yin, X. X.,& Wu, K. Half mode substrate integrated waveguide: A new guided wave structure for microwave and millimeter wave application. In Joint 31st International Conference on Infrared Millimeter Waves and 14th International Conference on Teraherz Electronics, 2006, (pp. 219-219). IEEE.
9. Nguyen-Trong, N., &Fumeaux, C. Half-mode substrate-integrated waveguides and their applications for antenna technology: A review of the possibilities for antenna design. IEEE Antennas and Propagation Magazine, 2018, 60(6), 20-31.
10. Cassivi, Y., Perregrini, L., Arcioni, P., Bressan, M., Wu, K., &Conciauro, G. Dispersion characteristics of substrate integrated rectangular waveguide. IEEE Microwave and Wireless components letters, 2002, 12(9), 333-335.
11. Bochra, R., Mohammed, F., & Tao. J. Design of optimal chamfered bends in Rectangular Substrate Integrated Waveguide. International Journal of Computer Science Issues (IJCSI), 2011, 8(4).
12. Rahali, B., &Feham, M. Coupler, Power Divider and Circulator in V-Band Substrate Integrated Waveguide Technology. IJCSA International Journal on Computational Sciences & Applications, 2013, 3(6).
13. Rahali, B., & Feham, M. Design of K-Band substrate integrated waveguide coupler, circulator and power divider. International Journal of Information and Electronics Engineering, 2014, 4(1), 47.
14. Hamzah, A. M., Audah, L., &Alkhafaji, N. H-shaped fractal slots based highly miniaturized substrate integrated waveguide metamaterialbandpass filters for C-band applications. Progress In Electromagnetics Research B, 2020, 86, 139-158.
15. Khanna, G., & Sharma, N. Fractal antenna geometries: A review. International Journal of Computer Applications, 2016, 153(7), 29-32.
16. Khanna, G., &Sharma.Fractal antenna geometries: A review. International Journal of Computer Applications, 2016, 153(7), 29-32.
17. Pozar, D. M. Microstrip antennas. Proceedings of the IEEE.1992, 802019 (1). 79-91.
18. High Frequency Structure Simulator software package, HFSS v13, Ansoft Corporation
19. Fesharaki, F., Djerafi, T., Chaker, M., & Wu, K. S-parameter deembedding algorithm and its application to substrate integrated waveguide lumped circuit model extraction. IEEE Transactions on Microwave Theory and Techniques, 2017, 65(4).

20. Deslandes, D., & Wu, K. Integrated microstrip and rectangular waveguide in planar form. IEEE microwave and wireless components letters, 2001, 11(2), 68-70.
21. Deslandes, D., & Wu, K. Analysis and design of current probe transition from grounded coplanar to substrate integrated rectangular waveguides. IEEE transactions on microwave theory and techniques, 2005, 53(8).
22. Deslandes, D. Design equations for tapered microstrip-to-substrate integrated waveguide transitions. In IEEE MTT-S International Microwave Symposium. 2010, (pp. 704-707).IEEE.
23. Ding, Y., & Wu, K. Substrate integrated waveguide-to-microstrip transition in multilayer substrate. IEEE Transactions on Microwave Theory and Techniques, 2007, 55(12) .
24. Deslandes, D., & Wu, K. Integrated transition of coplanar to rectangular waveguides. In IEEE MTT-S International Microwave Sympsoium Digest (Cat. No. 01CH37157), 2001, Vol. 2, pp. 619-622.
25. Xia, L., Xu, R., Yan, B., Li, J., Guo, Y. C., & Wang, J. Broadband transition between air-filled waveguide and substrate integrated waveguide. Electronics letters, 2006, 42(24).
26. Goswami, L. P., Sarkar, A., &Biswas, A. Design and implementation of SIW based multiple output X-band phase shifters. In 2016 Asia-Pacific Microwave Conference (APMC), 2016, pp. 1-4.IEEE.
27. Lyu, Y. P., Zhu, L., & Cheng, C. H. Synthesis design of filtering wideband differential phase shifters on multimode resonators with controllable same insertion loss bandwidth. IET Microwaves, Antennas & Propagation, 2018, 12(3).
28. Lyu, Y. P., Zhu, L., & Cheng, C. H. A new design of ultrawideband single-layer 90° phase shifter in the view of group delay. IEEE Microwave and Wireless Components Letters, 2019, 29(6), 376-378.
29. Qiu, L. L., Zhu, L., &Lyu, Y. P. Balanced wideband phase shifters with wide phase shift range and good common-mode suppression. IEEE Transactions on Microwave Theory and Techniques, 2019, 67(8).
30. Chaudhary, G., &Jeong, Y. Wideband tunable differential phase shifter with minimized in-band phase deviation error. IEEE Microwave and Wireless Components Letters, 2019, 29(7), 468-470.
31. Yoon, H. J., & Min, B. W. Wideband 180° phase shifter using parallel-coupled three-line. IEEE Microwave and Wireless Components Letters, 2019, 29(2), 89-91.
32. Rahimian, Z., Gigoyan, S., Pourziad, A., Nikmehr, S., & Safavi-Naeini, S. Two-way phase shifter with equal phase shift. In IEEE International Symposium on Antennas and Propagation and USNC-URSI Radio Science Meeting, 2019, pp. 995-996. .
33. Liu, S., &Xu, F. Novel substrate-integrated waveguide phase shifter and its application to six-port junction. IEEE Transactions on Microwave Theory and Techniques, 2019, 67(10), 4167-4174..
34. Der, E. T., Jones, T. R., &Daneshmand, M. Miniaturized tunable phase shifter using a periodically loaded ridged half-mode substrate integrated waveguide. In 2019 IEEE MTT-S International Microwave Symposium (IMS),2019, pp. 180-183.
35. Der, E. T., Jones, T. R., &Daneshmand, M. Miniaturized 4× 4 Butler matrix and tunable phase shifter using ridged half-mode substrate integrated waveguide. IEEE Transactions on Microwave Theory and Techniques, 2020, 68(8).
36. Omam, Z. R., Abdel-Wahab, W. M., Pourziad, A., Nikmehr, S., Palizban, A., Gigoyan, S., & Safavi-Naeini, S. Tunable substrate integrated waveguide phase shifter using high dielectric constant slab. IEEE Microwave and Wireless Components Letters, 2020, 30(5), 485-488.
37. Zhao, C., &Fumeaux, C. Beam-steerable phased antenna arrays using substrate-integrated waveguide phase shifters. In 13th European Conference on Antennas and Propagation (EuCAP),2019, pp. 1-4.
38. Kumari, G., Barik, R. K., Saxena, P., & Karthikeyan, S. S. Compact substrate integrated waveguide power divider with slot-loaded ground plane for dual-band applications. In 2018 IEEE MTT-S International Microwave and RF Conference (IMaRC), 2018, pp. 1-4.
39. Danaeian, M., Moznebi, A. R., Afrooz, K., & Hakimi, A. Miniaturized filtering SIW power divider with arbitrary power-dividing ratio loaded by open complementary split-ring resonators. International Journal of Microwave and Wireless Technologies, 2017, 9(9).
40. Kumar, A., Murugeshwari, B., & Raghavan, S. Design of substrate integrated waveguide power divider and parameter optimization using neural network. IOSR Journal of Electronics and Communication Engineering (IOSR-JECE), 2018, 13(1), 37-43.
41. Song, K., Luo, M., Yao, J., & Zhou, Y. Dual-pass band-band pass-filtering power divider using half-mode substrate integrated waveguide resonator with high frequency selectivity. International Journal of RF and Microwave Computer-Aided Engineering, 2020, 30(9).
42. Hussein, O., Al Shamaileh, K., Sigmarsson, H., Abushamleh, S., Aboserwal, N., & Devabhaktuni, V. A half-mode substrate integrated waveguide filtering power divider with Fourier-varying via holes. Microwave and Optical Technology Letters, 2021, 63(12), 2964-2968.
43. Djerafi, T., Hammou, D., Wu, K., &Tatu, S. O. Ring-shaped substrate integrated waveguide Wilkinson power dividers/combiners. IEEE transactions on components, packaging and manufacturing technology, 2014, 4(9).
44. Moulay, A., &Djerafi, T. Wilkinson power divider with fixed width substrate-integrated waveguide line and a distributed isolation resistance. IEEE Microwave and Wireless Components Letters, 2018, 28(2), 114-116.
45. Distributed Isolation Resistance, IEEE Microwave and wireless components letters. IEEE. Personal use is permitted, but republication/redistribution requires IEEE permission, 2018.
46. Chaturvedi, D., Kumar, A., & Raghavan, S. An integrated SIW cavity-backed slot antenna-triplexer. IEEE Antennas and Wireless Propagation Letters, 2018, 17(8).

47. Mukherjee, S., Biswas, A., &Srivastava, K. V. Substrate integrated waveguide cavity-backed dumbbell-shaped slot antenna for dual-frequency applications. IEEE Antennas and Wireless Propagation Letters, 14, 2014.
48. Jones, T. R., &Daneshmand, M. Miniaturized slotted bandpass filter design using a ridged half-mode substrate integrated waveguide. IEEE Microwave and Wireless Components Letters, 2016, 26(5), 334-336.
49. Yang, Q. L., Ban, Y. L., Lian, J. W., Yu, Z. F., & Wu, B. SIW butler matrix with modified hybrid coupler for slot antenna array, 2016.
50. Zhang, W., Shen, Z., Xu, K., & Shi, J. A compact wideband phase shifter using slotted substrate integrated waveguide. IEEE Microwave and Wireless Components Letters, 2019, 29(12), 767-770.
51. Mbaye, M., Hautcoeur, J., Talbi, L., &Hettak, K. Bandwidth broadening of dual-slot antenna using substrate integrated waveguide (SIW). IEEE Antennas and Wireless Propagation Letters, 12.2013.
52. Jawad, M. M., Abd Malik, N. N. N., Murad, N. A., Esa, M. R. M., Ahmad, M. R., Mekki, A. S., ...& Hussein, Y. M. Implantable slot antenna with substrate integrated waveguide for biomedical applications. Telkomnika, 2021, 19(5).
53. Balanis, C. A. Antenna theory: analysis and design. John wiley& sons, 2015.
54. Werner, D. H., Haupt, R. L., & Werner, P. L. Fractal antenna engineering: The theory and design of fractal antenna arrays. IEEE Antennas and propagation Magazine, 1999, 41(5), 37-58.
55. Kharat, K., Dhoot, S., &Vajpai, J. Design of compact multiband fractal antenna for WLAN and WiMAX applications. In International Conference on Pervasive Computing (ICPC) ,2015, pp. 1-4. IEEE.
56. Singh, M., & Sharma, N. A design of star shaped fractal antenna for wireless applications. International Journal of Computer Applications, 2016, 134(4), 41-43.
57. Chen, H. Research into the fundamental mode and high order mode of koch island fractal antenna, Shipboard Electronic Countermeasure, 2014.
58. Islam, Z. U., Rahman, M., Muhammad, N., Ahmed, Z., Lodhi, F. K., &Haneef, M. Dual band second order modified Sierpinski monopole reduced size fractal antenna. In International Conference on Emerging Technologies (ICET), 2016, pp. 1-5.
59. Choudhury, S., & Mohan, A. MiNiaturized quarter-mode substrate integrated waveguide (QMSIW) antenna using Sierpinski fractal geometry. In Asia-Pacific Microwave Conference (APMC), 2016, pp. 1-4.
60. Mondal, T., Suman, S., & Singh, S. Novel Design of Fern Fractal Based Triangular Patch Antenna. In 2020 National Conference on Emerging Trends on Sustainable Technology and Engineering Applications (NCETSTEA) ,2020, pp. 1-3.
61. Kumar, A., &Raghavan, S. A review: substrate integrated waveguide antennas and arrays. Journal of Telecommunication, Electronic and Computer Engineering (JTEC), 2016, 8(5), 95-104.
62. Kumar, A., &Raghavan, S. A review: substrate integrated waveguide antennas and arrays. Journal of Telecommunication, Electronic and Computer Engineering (JTEC), 2016, 8(5), 95-104.
63. Alieldin, A., Huang, Y., Stanley, M., Joseph, S. D., & Lei, D. A 5G MIMO antenna for broadcast and traffic communication topologies based on pseudo inverse synthesis. , 6, 2018.
64. Gao, Y., Khaliel, M., Zheng, F., & Kaiser, T. Rotman lens based hybrid analog–digital beamforming in massive MIMO systems: Array architectures, beam selection algorithms and experiments. IEEE Transactions on Vehicular Technology, 2017, 66(10).
65. Santhakumar, G., Vadivelu, R., Lakshmi, M. R., Saranya, G. J., &Subasini, R. Design of Substrate-Integrated-Waveguide Antenna for Automotive Short Range Radar Application. In 7th International Conference on Advanced Computing and Communication Systems (ICACCS), 2021, Vol. 1, pp. 707-710.
66. Saad, A. A. R., & Mohamed, H. A. Bandwidth enlargement of a low-profile open-ring slot antenna based on SIW structure. IEEE Antennas and Wireless Propagation Letters.2017.